Specific and Nonhepatotoxic Degradation of Nuclear Hepatitis B Virus cccDNA

Julie Lucifora *et al.*

Science **343**, 1221 (2014);
DOI: 10.1126/science.1243462

Science (print ISSN 0036-8075; online ISSN 1095-9203) is published weekly, except the last week in December, by the American Association for the Advancement of Science, 1200 New York Avenue NW, Washington, DC 20005.

Specific and Nonhepatotoxic Degradation of Nuclear Hepatitis B Virus cccDNA

Julie Lucifora,[1,2]* Yuchen Xia,[1]* Florian Reisinger,[1] Ke Zhang,[1] Daniela Stadler,[1] Xiaoming Cheng,[1] Martin F. Sprinzl,[1,3] Herwig Koppensteiner,[1] Zuzanna Makowska,[4] Tassilo Volz,[5] Caroline Remouchamps,[6] Wen-Min Chou,[1] Wolfgang E. Thasler,[7] Norbert Hüser,[8] David Durantel,[9] T. Jake Liang,[10] Carsten Münk,[11] Markus H. Heim,[4] Jeffrey L. Browning,[12] Emmanuel Dejardin,[6] Maura Dandri,[2,5] Michael Schindler,[1] Mathias Heikenwalder,[1]†‡ Ulrike Protzer[1,2]†‡

Current antiviral agents can control but not eliminate hepatitis B virus (HBV), because HBV establishes a stable nuclear covalently closed circular DNA (cccDNA). Interferon-α treatment can clear HBV but is limited by systemic side effects. We describe how interferon-α can induce specific degradation of the nuclear viral DNA without hepatotoxicity and propose lymphotoxin-β receptor activation as a therapeutic alternative. Interferon-α and lymphotoxin-β receptor activation up-regulated APOBEC3A and APOBEC3B cytidine deaminases, respectively, in HBV-infected cells, primary hepatocytes, and human liver needle biopsies. HBV core protein mediated the interaction with nuclear cccDNA, resulting in cytidine deamination, apurinic/apyrimidinic site formation, and finally cccDNA degradation that prevented HBV reactivation. Genomic DNA was not affected. Thus, inducing nuclear deaminases—for example, by lymphotoxin-β receptor activation—allows the development of new therapeutics that, in combination with existing antivirals, may cure hepatitis B.

Hepatitis B virus (HBV) infection remains a major public health threat, with more than 350 million humans chronically infected worldwide at risk of developing end-stage liver disease and hepatocellular carcinoma. Each year, more than 600,000 people die from the consequences of chronic HBV infection. A prophylactic vaccine has been available for hepatitis B for almost 30 years, but the overall number of chronic infections remains high.

HBV is a small, enveloped DNA virus replicating via an RNA intermediate. The encapsidated viral genome consists of a 3.2-kb partially double-stranded relaxed circular DNA (rcDNA) molecule. The virus has optimized its life cycle for long-term persistence in the liver (*1*). Upon translocation to the nucleus, the rcDNA genome is converted into a covalently closed circular DNA (cccDNA), which serves as the template for viral transcription and secures HBV persistence. Nucleoside or nucleotide analogs are efficient antivirals but only control and do not cure HBV infection owing to the persistence of HBV cccDNA. Therefore, long-term treatment is required, which is expensive and may lead to concomitant resistance (*2*). Interferon (IFN)–α is licensed for hepatitis B therapy, and treatment with this cytokine can result in virus clearance in a proportion of patients; however, its efficacy is limited and high doses are not tolerated (*3*). Thus, efficient and nontoxic elimination of cccDNA in hepatocytes is a major goal of HBV research.

Using animal models, it has been shown that HBV replication—in particular, the cccDNA content of the liver—can be affected by noncytopathic mechanisms involving cytokines such as interferons and tumor necrosis factor (TNF), which influence RNA and capsid stability (*4*–*7*). Here, we describe an antiviral mechanism that interferes with cccDNA stability and is distinct from influences of antiviral cytokines on cccDNA activity (*8*).

High-Dose IFN-α Leads to cccDNA Degradation in HBV-Infected Hepatocytes

IFN-α is known to exert transcriptional, post-transcriptional, and epigenetic antiviral effects on HBV (*8*–*12*). To study the effect of IFN-α on HBV cccDNA, we used HBV-infected, differentiated HepaRG (dHepaRG) cells and primary human hepatocytes (PHHs). These are human cell types susceptible to HBV infection (*13*, *14*) and responsive to IFN-α treatment in vitro (fig. S1A). IFN-α treatment did not lead to detectable hepatotoxicity, even at very high doses (fig. S1B). Treating dHepaRG cells with IFN-α (500 or 1000 IU/ml) controlled HBV-DNA synthesis as efficiently as the nucleoside analog lamivudine (LAM) at 0.5 μM (5 times the median effective concentration, EC_{50}). IFN-α, however, unlike LAM, also significantly reduced expression of HBV-RNA and hepatitis B surface (HBsAg) and e (HBeAg) antigens (Fig. 1A and fig. S1C).

In patients, interruption of LAM treatment results in a rebound of HBV replication (*2*). Using IFN-α, we observed only a partial rebound, or none at all, in HBV-infected dHepaRG cells after treatment cessation (Fig. 1A). Because dHepaRG cells do not allow virus spread, reduction of HBeAg and the lack of rebound indicated an effect of IFN-α on the established HBV cccDNA transcription template separate from the known antiviral effects on viral replication (*14*). By cccDNA-specific quantitative polymerase chain reaction (qPCR), we determined an 80% reduction of cccDNA after 10 days of treatment (Fig. 1B). Reduction of cccDNA was confirmed by Southern blot analysis (fig. S1D) and was dose-dependent (fig. S1E). cccDNA reduction could be induced at any time point (Fig. 1C) and persisted over time (Fig. 1, A and C). The effect was corroborated in HBV-infected PHHs (Fig. 1D). In contrast to IFN-α, LAM and the even more potent nucleoside analog entecavir (ETV) at very high doses (0.5 μM; 1000 times EC_{50}) only inhibited reverse transcription, and thus HBV replication, but not viral persistence (Fig. 1E). Pretreatment with ETV did not enhance the effect of IFN-α (Fig. 1F), indicating that IFN-α induces the decay of established HBV cccDNA. Because the doses of IFN-α used to achieve this effect were high, we screened for other cytokines showing similar antiviral effects at moderate doses.

LTβR Activation Controls HBV and Leads to cccDNA Degradation in HBV-Infected Cells

IFN-γ and TNF-α are known to control HBV in a noncytopathic fashion (*4*, *7*) but cannot be used as therapeutics because they cause severe side effects. We tested the effect of lymphotoxin (LT) β receptor (LTβR) activation as an alternative therapeutic option. The TNF superfamily members LTα, LTβ, and CD258 are the physiological ligands for LTβR and activate either inflammatory or anti-inflammatory pathways or induce apoptosis (*15*). Like hepatocytes (*16*), dHepaRG (*14*) and HepG2-H1.3 cells permit HBV replication (*17*) and express LTβR (fig. S2, A and B). To activate LTβR, we used a superagonistic tetravalent bispecific antibody (BS1) and a bivalent anti-LTβR monoclonal antibody (CBE11) (*18*, *19*). As expected, LTβR agonists activated canonical (*20*) and noncanonical nuclear factor κB (NF-κB) pathways to trigger p100 cleavage (fig. S2C), RelA phosphorylation (fig. S2D), nuclear RelB and RelA translocation (fig. S2, E and F), and up-regulation of known target genes (fig. S2G) without causing any detectable hepatocytotoxicity (fig. S2H).

[1]Institute of Virology, Technische Universität München–Helmholtz Zentrum München, 81675 Munich, Germany. [2]German Center for Infection Research (DZIF), Munich and Hamburg sites, Germany. [3]1st Medical Department, University Hospital Mainz, 55131 Mainz, Germany. [4]Department of Biomedicine, University Hospital Basel, 4031 Basel, Switzerland. [5]Department of Internal Medicine, University Medical Center Hamburg-Eppendorf, 20246 Hamburg, Germany. [6]GIGA-Research Laboratory of Molecular Immunology and Signal Transduction, University of Liège, 4000 Liège, Belgium. [7]Department of General, Visceral, Transplantation, Vascular and Thoracic Surgery, Grosshadern Hospital, Ludwig Maximilians University, 81377 Munich, Germany. [8]Department of Surgery, University Hospital Rechts der Isar, Technische Universität München, 85748 Munich, Germany. [9]INSERM U1052, CNRS UMR 5286, Cancer Research Center of Lyon, University of Lyon, LabEx DEVweCAN, 69007 Lyon, France. [10]Liver Diseases Branch, National Institute of Diabetes and Digestive and Kidney Diseases, Bethesda, MD 20892, USA. [11]Clinic for Gastroenterology, Hepatology and Infectiology, Medical Faculty, Heinrich-Heine University, 40225 Düsseldorf, Germany. [12]Department of Immunobiology, Biogen Idec, Cambridge, MA 02142, USA.

*These authors contributed equally to this work.
†Corresponding author. E-mail: protzer@tum.de (U.P.); heikenwaelder@helmholtz-muenchen.de (M.H.)
‡These authors contributed equally to this work.

To test the effect of LTβR activation on HBV infection, we treated dHepaRG cells with BS1 for 12 days starting 24 hours before HBV infection. LTβR activation decreased levels of all HBV markers, including cccDNA, by ~90% without toxicity (Fig. 2A). The antiviral effect was highly potent, with an EC_{50} of ~0.01 μg/ml (fig. S3A). Inhibition of apoptosis did not alter antiviral activity (fig. S4). Neither IFN-β nor representative IFN-stimulated genes were upregulated upon BS1 treatment (fig. S2G), and antiviral activity was independent of IFN induction (fig. S5).

In vivo, activation of the murine LTβR by systemic application of an agonistic antibody (ACH6) induced RelA and RelB nuclear translocation in hepatocytes of HBV-transgenic mice (fig. S6A) and reduced HBV viremia (fig. S6B), HBV RNA (fig. S6C), and HBV core (HBc) protein expression in the liver (fig. S6, D and E). Neither signs of hepatocyte apoptosis (fig. S6F) nor elevation of aminotransferases (ALT) (fig. S6G, right panel) were observed, indicating good in vivo tolerability of LTβR activation. Because HBV-transgenic mice do not establish HBV cccDNA, this indicated additional antiviral effects of LTβR activation on HBV RNA transcription or stability. Accordingly, discontinuation of LTβR activation induced an immediate, strong rebound of HBV replication (fig. S6G).

To investigate whether LTβR activation would affect established HBV cccDNA in the context of a persistent infection and prevent HBV reactivation, we treated dHepaRG cells with LTβR agonists BS1 or CBE11 when a stable, nuclear cccDNA pool had established. All HBV markers, including HBV cccDNA, were reduced upon LTβR activation in HBV-infected dHepaRG cells (Fig. 2, B and C, and fig. S3) as well as in stably transfected HepG2-H1.3 cells containing high levels of cccDNA (Fig. 2C). In HBV-infected PHHs, LTβR agonization reduced HBV cccDNA, HBeAg secretion, and—most effectively—HBV-DNA replication (Fig. 2D). cccDNA degradation was more effective (up to 95%) when treatment was prolonged (fig. S3, C and D). Treatment interruption for 10 days was almost as efficient as continuous treatment (fig. S3C), indicating that LTβR agonists

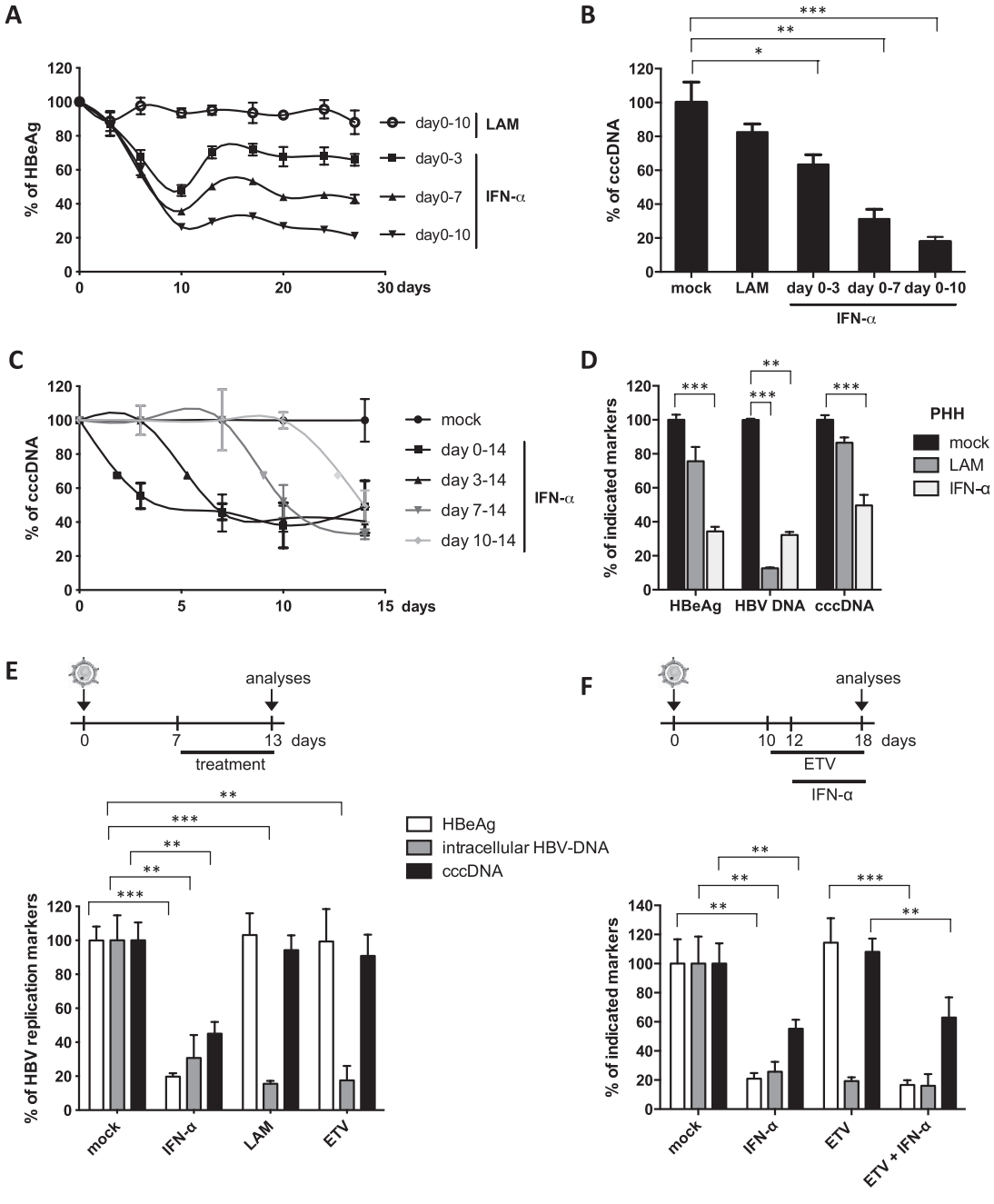

Fig. 1. Degradation of cccDNA in IFN-α–treated HepaRG cells and primary human hepatocytes. (**A**, **B**, **C**, **E**, and **F**) HBV-infected dHepaRG cells were treated with IFN-α at day 10 post-infection (dpi). Different regimens of treatment were applied as indicated. (**D**) HBV-infected PHHs were treated with IFN-α at dpi 3 for 13 days. Levels of HBeAg, total intracellular DNA, and cccDNA are given relative to mock-treated cells. LAM, lamivudine; ETV, entecavir. Data are means ± SD of replicates from independent experiments and were analyzed by *t* test. **P* < 0.05, ***P* < 0.01, ****P* < 0.001.

induce a persistent antiviral effect. In contrast to LAM treatment, no rebound of HBV replication was observed when BS1 treatment stopped (Fig. 2E). Hence, LTβR activation not only suppressed HBV replication but also caused nuclear cccDNA degradation, which is needed to achieve virus elimination.

LTβR Activation and IFN-α Treatment Induce Deamination and Apurinic/Apyrimidinic (AP) Site Formation in cccDNA

To investigate whether cccDNA degradation upon LTβR activation or IFN-α treatment was a result of DNA damage, we examined cccDNA deamination by differential DNA denaturation PCR (3D-PCR) (*21*). Lower denaturing temperatures were sufficient for cccDNA amplification from HBV-infected dHepaRG cells and for PHHs treated with IFN-α or BS1, compared with denaturing temperatures needed to amplify cccDNA from untreated, LAM-treated, or ETV-treated cells (Fig. 3A and fig. S7, C and D). Using a cocktail of recombinant proteins containing all enzymes necessary for DNA repair, we could reverse the denaturation of cccDNA (Fig. 3A, lower panels). The fact that the denaturation temperatures of mock-, LAM-, and ETV-treated cells also shifted indicated that this modification of HBV cccDNA existed even without exposure to exogenous drugs. Deamination of cccDNA (Fig. 3A, right panel) and a drop in cccDNA levels after treatment with CBE11 (table S1) were confirmed in vivo in human liver chimeric uPA-SCID mice infected with HBV. Sequencing analyses showed that G→A transitions occurred under treatment (Fig. 3B and fig. S7, A and B), indicating deamination of cytidines to uridine in the HBV cccDNA minus strand. At lower denaturation temperatures, G→A transitions became more obvious (Fig. 3C and fig. S7A). These data showed that both LTβR activation and IFN-α treatment led to cccDNA deamination in vitro and in vivo, and help to explain the G→A hypermutation observed in patient samples (*21*).

Neither deamination nor mutations of genomic DNA were observed by 3D-PCR (fig. S8A) or by deep sequencing of selected housekeeping genes or of IFN and LTβR target genes (fig. S8B). This finding indicated that DNA modifications were specifically targeted to viral cccDNA.

After cytidine deamination, DNA glycosylases recognize the damaged DNA and cleave N-glycosidic bonds to release the base and create an accessible apurinic/apyrimidinic site (AP site) that can then be cleaved by endonucleases (*22*). These AP sites can be repaired, can lead to mutations upon DNA replication, or can induce DNA degradation (*23*). We quantified AP sites created by LTβR activation or IFN-α treatment. However, no increase of AP sites in total DNA extracts from dHepaRG cells or PHHs treated with IFN-α or LTβR agonists (fig. S8C) was found, indicating again that our treatments did not lead to detectable damage in genomic DNA. Because AP sites in the small (3.2 kb) cccDNA are very likely to be missed by this analysis, we digested total DNA extracts with an AP endonuclease (APE1) and then amplified cccDNA by qPCR. APE digestion further decreased cccDNA extracted from dHepaRG cells and PHHs treated with IFN-α or LTβR agonists but not with LAM (Fig. 3D). Taken together, our data indicate that both LTβR activation and IFN-α treatment induced deamination and AP site formation in HBV cccDNA, leading to its degradation, but did not affect genomic DNA.

LTβR Activation and IFN-α Treatment Up-Regulate Expression of Nuclear APOBEC3 Deaminases

IFN-α is known to induce several cytidine deaminases (*23*, *24*). We performed genome-wide expression profiling of HBV-infected dHepaRG

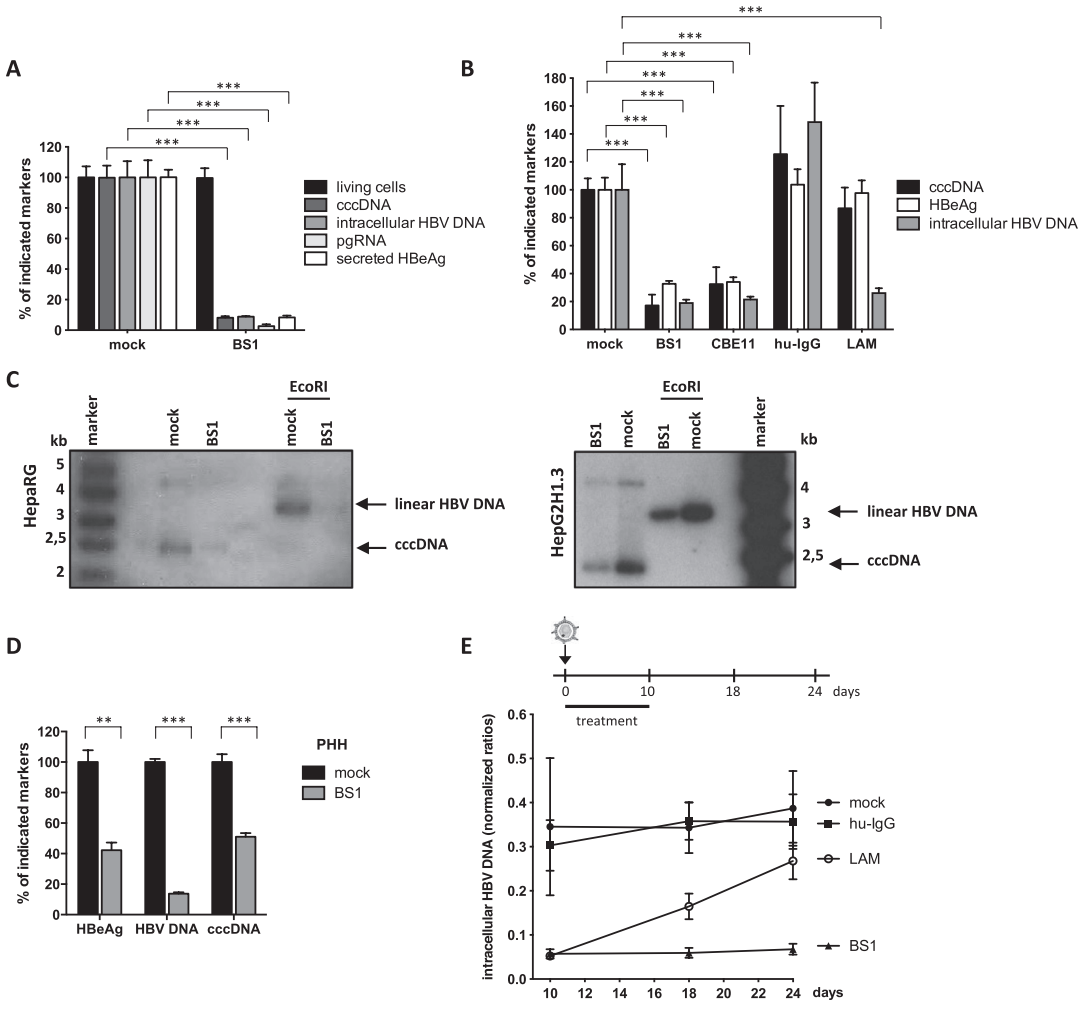

Fig. 2. LTβR activation inhibits HBV infection and leads to cccDNA degradation in HepaRG cells and PHHs. (**A** and **B**) HBV-infected dHepaRG cells were treated with BS1, CBE11, human immunoglobulin (hu-IgG) control, or lamivudine (LAM). Treatment started 24 hours before infection for 12 days (A) or at 18 dpi for 10 days (B). Levels of the indicated HBV markers as well as cell viability are given relative to untreated controls (mock). (**C**) cccDNA levels were analyzed after 14 days of BS1 treatment by Southern blot in HBV-infected dHepaRG and HBV-replicating HepG2-H1.3 cells. Supercoiled cccDNA bands were identified by their expected size and linearization upon Eco RI digestion (3.2 kb). (**D**) PHHs were infected with HBV and treated with BS1 at 7 dpi for 10 days. Levels of the indicated HBV markers were compared to untreated PHHs of the same donor (donor 3) (mock). (**E**) HBV-infected dHepaRG cells were treated with BS1, hu-IgG control, or LAM. Intracellular HBV-DNA was analyzed 8 and 14 days after treatment cessation. Data are means ± SD of replicates from independent experiments and were analyzed by *t* test. $^{*}P < 0.05$, $^{**}P < 0.01$, $^{***}P < 0.001$.

cells after LTβR activation (fig. S9A) and classified regulated genes according to their activity and properties (fig. S9B). The gene encoding APOBEC3B (A3B) was identified as the most up-regulated gene with nucleic acid–binding properties (fig. S9C).

Analysis of all APOBEC3 family members showed that LTβR activation leads to strong up-regulation of A3B, and to a lesser extent A3G, in HBV-infected dHepaRG cells and PHHs and after systemic application in human liver chimeric uPA-SCID mice (fig. S10A). A3B expression was induced by LTβR activation in a dose-dependent manner, and expression levels steadily increased during continuous treatment (fig. S11), correlating with a concomitant increase in treatment efficacy over time (fig. S3C). Treatment of PHHs isolated from different donors with the LTβR agonist BS1 resulted in cccDNA degradation at different levels (Fig. 3E and fig. S10B), which could be explained neither by the difference in the level of A3B up-regulation (Fig. 3E) nor by detection of a previously described (*25*) genomic deletion of the A3B allele, which seems to correlate with

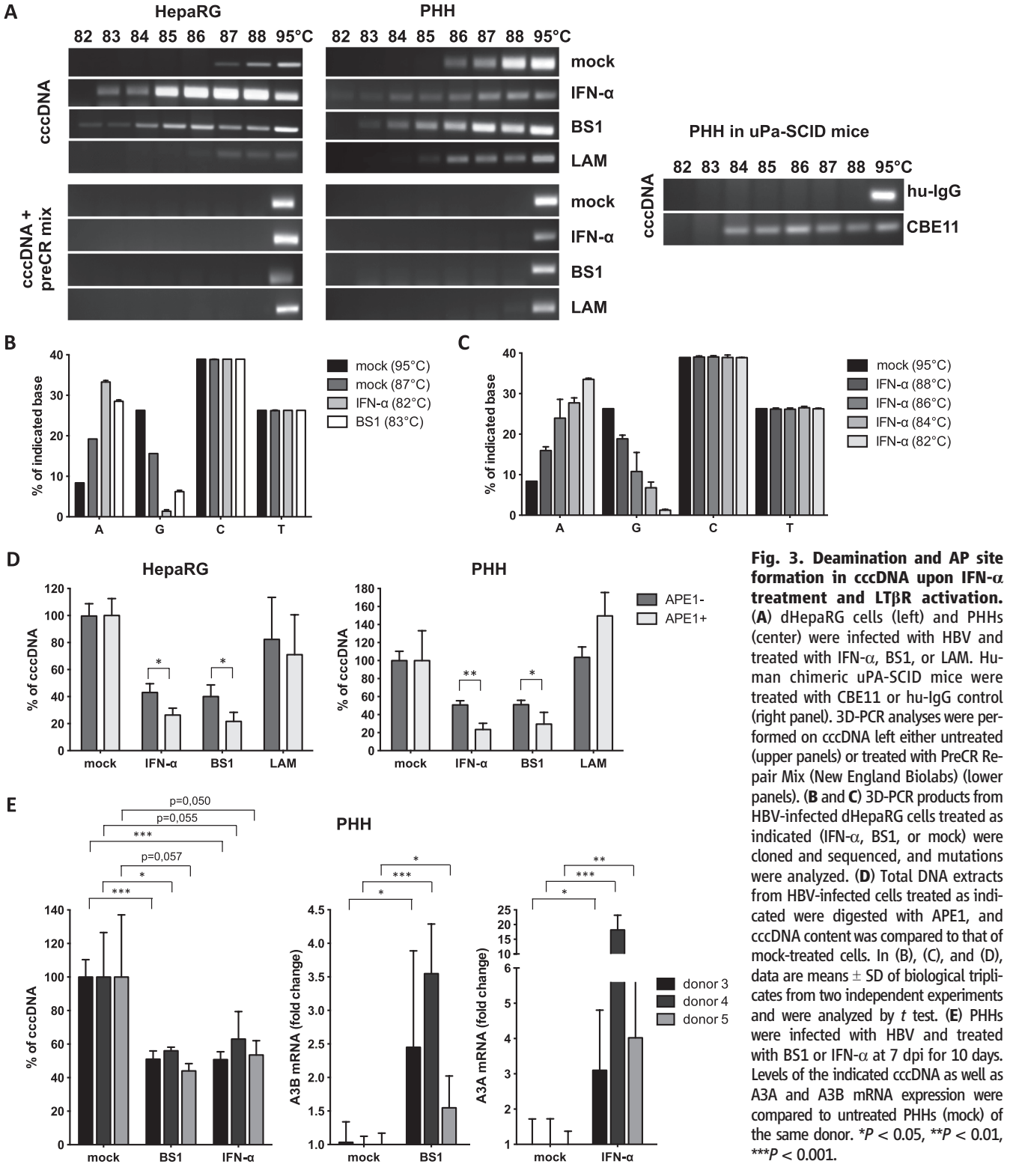

Fig. 3. Deamination and AP site formation in cccDNA upon IFN-α treatment and LTβR activation. (**A**) dHepaRG cells (left) and PHHs (center) were infected with HBV and treated with IFN-α, BS1, or LAM. Human chimeric uPA-SCID mice were treated with CBE11 or hu-IgG control (right panel). 3D-PCR analyses were performed on cccDNA left either untreated (upper panels) or treated with PreCR Repair Mix (New England Biolabs) (lower panels). (**B** and **C**) 3D-PCR products from HBV-infected dHepaRG cells treated as indicated (IFN-α, BS1, or mock) were cloned and sequenced, and mutations were analyzed. (**D**) Total DNA extracts from HBV-infected cells treated as indicated were digested with APE1, and cccDNA content was compared to that of mock-treated cells. In (B), (C), and (D), data are means ± SD of biological triplicates from two independent experiments and were analyzed by *t* test. (**E**) PHHs were infected with HBV and treated with BS1 or IFN-α at 7 dpi for 10 days. Levels of the indicated cccDNA as well as A3A and A3B mRNA expression were compared to untreated PHHs (mock) of the same donor. $*P < 0.05$, $**P < 0.01$, $***P < 0.001$.

HBV persistence in infected patients (fig. S10, B and C).

In contrast to LTβR activation, IFN-α treatment induced mainly A3A expression, as well as A3F and A3G expression, in HBV-infected dHepaRG cells and PHHs (fig. S12A) and A3D expression in isolated PHHs. By systemic IFN treatment of chimpanzees (*26*), A3A was strongly up-regulated in liver needle biopsies (fig. S12B). Activation of A3A, A3F, and A3G after IFN-α treatment was dose- and time-dependent and decreased after an initial peak despite continuous treatment, indicating that cells become refractory to IFN-α (fig. S13). In patients treated with subcutaneous pegylated IFN-α, needle biopsies obtained at different time points confirmed a rapid, strong up-regulation of A3A (and, to a lesser extent, A3G) in the liver, peaking at 16 hours after treatment (fig. S12C). Expression levels declined after this time point and remained low until day 6 after treatment, confirming a fast but transient induction of A3A by IFN-α treatment. The findings that IFN-α induced a transient A3A induction and that cells rapidly became refractory to IFN-α may account for the limited effect of IFN-α treatment in HBV-infected patients (*3*).

APOBEC3A or APOBEC3B Activity Is Essential to Induce cccDNA Degradation

Among the APOBEC3 family members up-regulated in our experiments, only A3A and A3B located to the nucleus (fig. S14), where they can gain access to cccDNA. To verify that they are indeed responsible for the induction of cccDNA degradation, we overexpressed the HIV-Vif protein [known to promote the degradation of all APOBEC3 proteins except A3B (*27*, *28*)] in dHepaRG cells in a tetracycline-regulated fashion. Expression of HIV-Vif reduced A3A, A3F, and A3G expression (fig. S15A), reverted IFN-α–induced cccDNA deamination, and prevented cccDNA degradation induced by IFN-α treatment (Fig. 4A). However, expression of HIV-Vif did not alter A3B levels (fig. S15B) and had no impact on cccDNA degradation by LTβR activation (fig. S15C). To specifically address the role of A3A or A3B in cccDNA degradation, we further knocked down A3A and A3B in dHepaRG cells under IFN-α or LTβR agonist treatment, respectively, and observed reduced cccDNA deamination (Fig. 4, B and C, left panels). Both A3A and A3B knockdown completely reverted cccDNA degradation but could not rescue the additional effect of IFN-α or LTβR activation on HBV replication (Fig. 4, B and C, right panels).

To confirm the impact of A3A and A3B on cccDNA deamination, we overexpressed A3A and A3B, respectively, in HBV-replicating HepG2-H1.3 cells (Fig. 4, D and E). Cytidine deamination of nuclear cccDNA by A3A and A3B is in accordance with other studies showing that both localize to the nucleus (*29*) and may be involved in the elimination of foreign DNA (*23*).

APOBEC3A Interacts with HBV Core Protein and Binds to cccDNA

APOBECs have evolved to restrict retroviral replication (*30*) as well as DNA transfer into cells. They are able to clear foreign nuclear DNA (*23*, *31*),

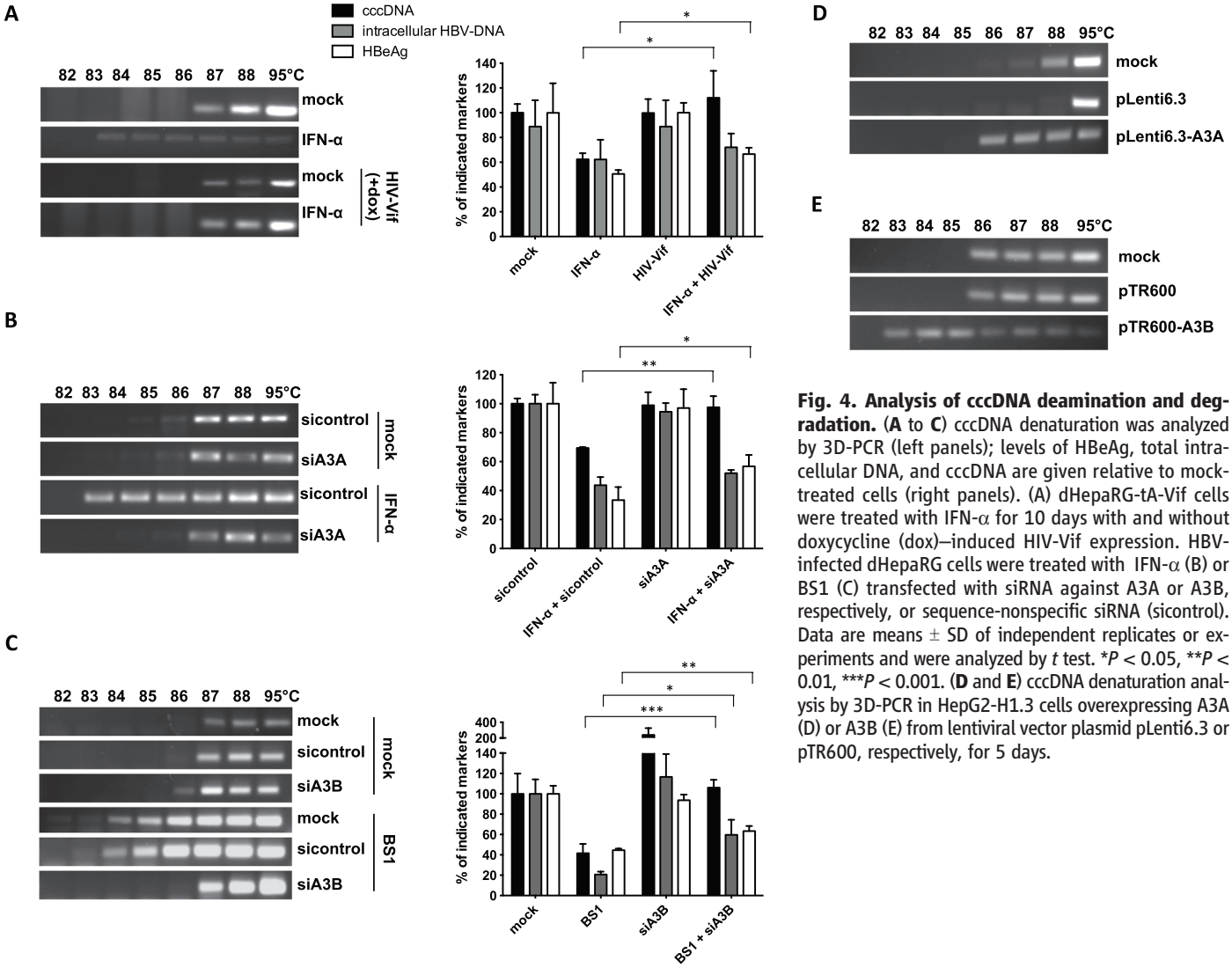

Fig. 4. Analysis of cccDNA deamination and degradation. (**A** to **C**) cccDNA denaturation was analyzed by 3D-PCR (left panels); levels of HBeAg, total intracellular DNA, and cccDNA are given relative to mock-treated cells (right panels). (A) dHepaRG-tA-Vif cells were treated with IFN-α for 10 days with and without doxycycline (dox)–induced HIV-Vif expression. HBV-infected dHepaRG cells were treated with IFN-α (B) or BS1 (C) transfected with siRNA against A3A or A3B, respectively, or sequence-nonspecific siRNA (sicontrol). Data are means ± SD of independent replicates or experiments and were analyzed by *t* test. $^{*}P < 0.05$, $^{**}P < 0.01$, $^{***}P < 0.001$. (**D** and **E**) cccDNA denaturation analysis by 3D-PCR in HepG2-H1.3 cells overexpressing A3A (D) or A3B (E) from lentiviral vector plasmid pLenti6.3 or pTR600, respectively, for 5 days.

but it remains unclear how HBV cccDNA was recognized and whether it was specifically targeted in our experiments. To assess specificity, we generated cell lines replicating a mammalian replicon plasmid pEpi containing a linear HBV 1.3× overlength sequence. From the linear HBV genome, HBV replication was initiated and, in addition to the pEpi-H1.3 replicon, HBV cccDNA was established in the nucleus. Treatment with either IFN-α or the LTβR agonist BS1 inhibited HBV replication and resulted in deamination and degradation of HBV cccDNA, but not of the HBV sequence–containing replicon (fig. S16). This result indicated that the deamination and subsequent degradation induced by both treatments is HBV cccDNA–specific.

HBV core protein associates with A3G (*32*) and HBV cccDNA (*33*) and was thus a candidate to mediate the targeting of A3 deaminases to HBV cccDNA. Confocal microscopy indicated a colocalization of A3A and A3B with the HBV core in different cell lines and PHHs (Fig. 5 and fig. S17). Chromatin immunoprecipitation (ChIP) experiments using stably (fig. S18A) or transiently transfected HepG2-H1.3 cells or HBV-infected and IFN-α treated dHepaRG cells showed that HBV core protein and A3A both bind to the cccDNA minichromosome (Fig. 6A). Supporting the possibility that a guardian protein prevents A3A direct binding to DNA (*34*), we could not detect A3A binding to genomic DNA (fig. S18B) even in the presence of the HBV core, which has been reported to also bind to cellular DNA (*35*).

HBV core protein coimmunoprecipitated A3A in HepG2-H1.3 cells and transfected HuH7 cells, indicating physical interaction with A3A (fig. S19). Proximity ligation assay (PLA) (Fig. 6B and fig. S20) and fluorescence resonance energy transfer (FRET) analysis (Fig. 6C) confirmed that the HBV core expressed after HBV infection directly interacted with A3A induced by IFN-α. By deletion analysis, we determined that the central region of HBc (amino acids 77 to 149) is involved in the interaction with A3A (Fig. 6C and fig. S21).

These data suggest that A3A may be targeted to cccDNA by interaction with the HBV core. No such targeting to genomic DNA has been described so far. Because APOBEC3 deaminases are thought to act on single-stranded DNA (*36*), one possibility is that A3A and A3B act on cccDNA when it is transiently rendered into single-stranded form by RNA polymerase II before transcription initiation.

We therefore suggest the following mechanism of APOBEC-dependent degradation of HBV cccDNA (Fig. 6D). High-dose IFN-α treatment or LTβR activation up-regulate the expression of A3A and A3B, respectively, which subsequently colocalize or directly interact with HBV core in infected hepatocytes and then translocate to the nucleus, where they are brought into close contact with cccDNA by the HBV core. The APOBECs can now deaminate cccDNA that is transiently rendered single-stranded during transcription. Uracils in HBV cccDNA are recognized and excised by cellular DNA glycosylases, leading to the formation of AP sites, which are then recognized by cellular AP endonucleases (*23*), leading in turn to cccDNA digestion. Why cccDNA is degraded instead of being repaired by the cellular DNA repair machinery has remained elusive. Using a mixture of various enzymes, we were able to repair deaminated cccDNA in tubo (Fig. 3A); this suggests the induction of an additional factor promoting DNA degradation or an impaired function of the repair machinery, rather than a lack of recognition by the repair machinery. Thus, we can only speculate that either (i) the number of AP sites introduced after treatment is too high and exceeds the capacity of the cellular repair machinery, or (ii) IFN-α treatment or LTβR activation [or even HBV itself (*37*)] modulates the repair machinery. This may shift the equilibrium from cccDNA repair (*38*) to degradation.

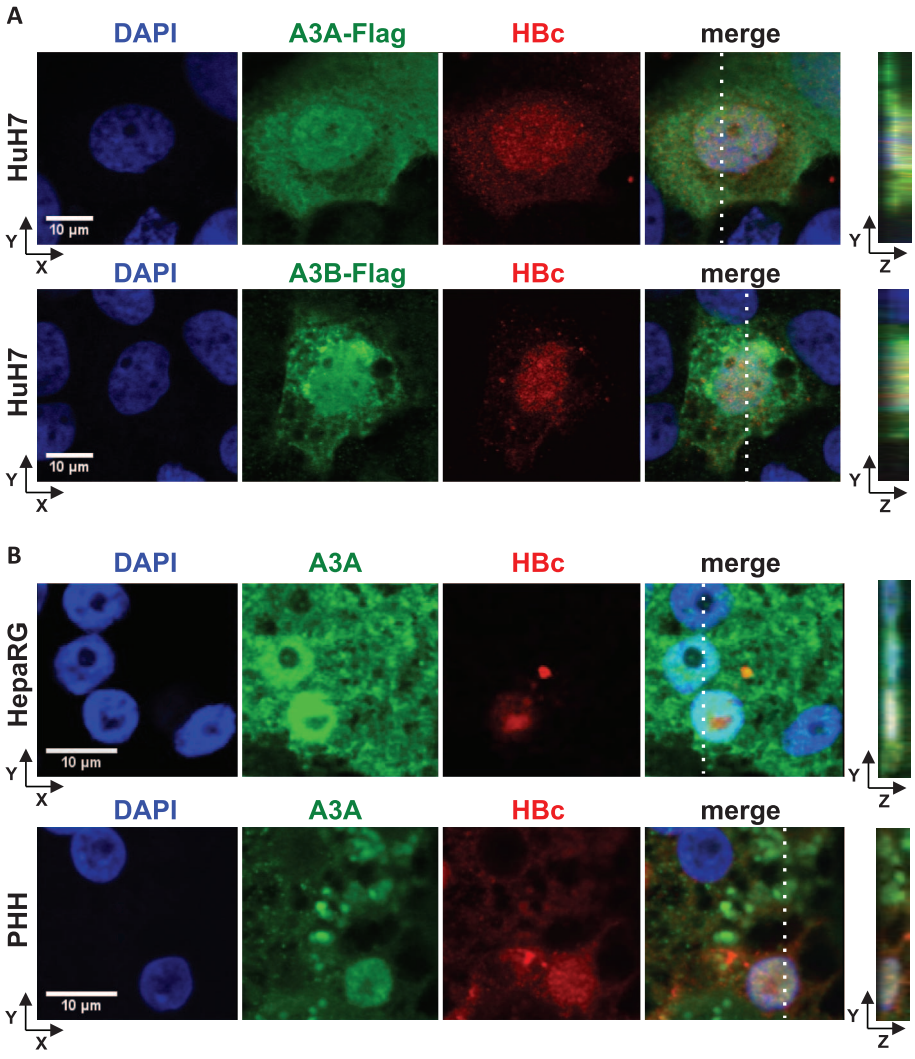

Fig. 5. Colocalization of A3A and A3B with HBV core protein (HBc). (**A**) HuH7 cells were cotransfected with an HBV 1.1× overlength genome and A3A-Flag– or A3B-Flag–expressing plasmids and stained using 4′,6-diamidino-2-phenylindole (DAPI) and antibodies to HBc and Flag. (**B**) HBV-infected dHepaRG cells and PHHs were treated with IFN-α at 7 dpi for 3 days. A3A and HBc were analyzed by immunofluorescence staining. Right panels indicate Z stacks taken at the dotted lines.

Ideally, a cure for HBV infection needs to eliminate cccDNA. Therefore, cytokines or cytokine receptor agonists that can trigger HBV cccDNA deamination and its degradation are interesting antiviral candidates. Antivirals that induce A3A and/or A3B activity should be combined with nucleoside or nucleotide analogs to avoid the replenishment of nuclear cccDNA after degradation. LTβR agonists were active at low doses, and we did not observe any toxicity in vitro or in vivo, nor did we detect any modification of genomic DNA. Constitutive overexpression of LTα/β for more than 1 year has been associated with inflammatory liver disease and hepatocellular carcinoma (*16*). As antivirals, however, LTβR agonists would be used for only a limited period of time, minimizing the risk of side effects. Moreover, LTβR activation has already been explored as a cancer treatment (*18*).

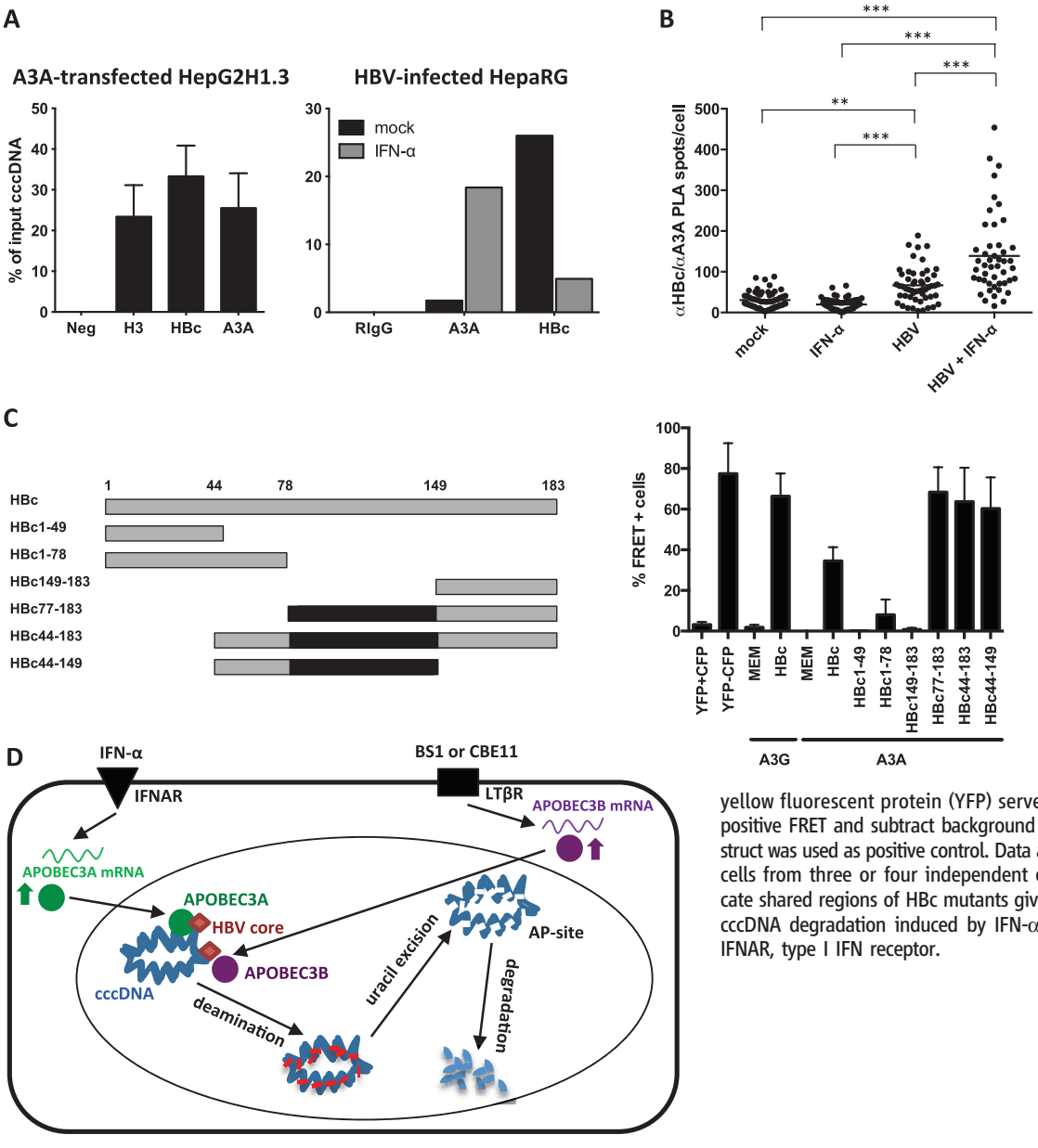

Fig. 6. Interaction of A3A, HBV core protein (HBc), and cccDNA. (**A**) Chromatin immunoprecipitation (ChIP) was performed using lysates of HepG2-H1.3 cells transfected with A3A-expressing plasmid or HBV-infected dHepaRG cells treated with IFN-α for 3 days. IPs using antibodies against histone H3, A3A, HBc, and control rabbit IgG (RIgG) were analyzed by qPCR for cccDNA. (**B**) Interaction between HBc and A3A was assessed by proximity ligation assay (PLA) in HBV-infected, IFN-α–treated dHepaRG cells. PLA spots were quantified in single cells by software-based spot counting. Data were analyzed by one-way analysis of variance. $^{**}P < 0.01$, $^{***}P < 0.001$. (**C**) Serial HBV core deletion mutants (left) were fused to cyan fluorescent protein (CFP), and interaction with A3A-YFP was assessed by fluorescence-activated cell sorting and FRET in HuH7.5 hepatoma cells (right). Cells cotransfected with CFP and yellow fluorescent protein (YFP) served as controls to exclude false positive FRET and subtract background signals. A CFP-YFP fusion construct was used as positive control. Data are means ± SD of FRET-positive cells from three or four independent experiments. Black boxes indicate shared regions of HBc mutants giving a FRET signal. (**D**) Model of cccDNA degradation induced by IFN-α treatment or LTβR activation. IFNAR, type I IFN receptor.

A recent study has shown a higher frequency of an A3B deletion allele in persistent HBV carriers and hepatocellular carcinoma patients relative to healthy controls (*25*). This finding was further supported by the moderate deamination of cccDNA even in the absence of treatment, and by the observation that knockdown of A3B in the absence of any treatment increased cccDNA levels. Although deregulated expression of A3A and A3B has been shown to correlate with genomic DNA mutations (*39*, *40*), we did not detect any alterations of genomic DNA using analyses of AP sites, 3D-PCR analysis, and deep sequencing of a set of human genes.

Our data indicate that cccDNA degradation is possible and can be induced without side effects on the infected host cell. An important task will be the testing of combinations of nucleoside or nucleotide analogs with novel antiviral strategies [e.g., LTβR agonists or adoptive T cell therapy (*41*)] to activate A3A or A3B to cure hepatitis B.

References and Notes

1. U. Protzer, M. K. Maini, P. A. Knolle, *Nat. Rev. Immunol.* **12**, 201–213 (2012).
2. F. Zoulim, *Liver Int.* **31** (suppl. 1), 111–116 (2011).
3. K. Wursthorn *et al.*, *Hepatology* **44**, 675–684 (2006).
4. L. G. Guidotti *et al.*, *Proc. Natl. Acad. Sci. U.S.A.* **91**, 3764–3768 (1994).
5. L. G. Guidotti *et al.*, *Science* **284**, 825–829 (1999).
6. S. F. Wieland, H. C. Spangenberg, R. Thimme, R. H. Purcell, F. V. Chisari, *Proc. Natl. Acad. Sci. U.S.A.* **101**, 2129–2134 (2004).
7. H. McClary, R. Koch, F. V. Chisari, L. G. Guidotti, *J. Virol.* **74**, 2255–2264 (2000).
8. L. Belloni *et al.*, *J. Clin. Invest.* **122**, 529–537 (2012).
9. A. Rang, S. Günther, H. Will, *J. Hepatol.* **31**, 791–799 (1999).
10. V. Pasquetto, S. F. Wieland, S. L. Uprichard, M. Tripodi, F. V. Chisari, *J. Virol.* **76**, 5646–5653 (2002).
11. S. F. Wieland, L. G. Guidotti, F. V. Chisari, *J. Virol.* **74**, 4165–4173 (2000).
12. S. L. Uprichard, S. F. Wieland, A. Althage, F. V. Chisari, *Proc. Natl. Acad. Sci. U.S.A.* **100**, 1310–1315 (2003).
13. P. Gripon *et al.*, *J. Virol.* **62**, 4136–4143 (1988).
14. P. Gripon *et al.*, *Proc. Natl. Acad. Sci. U.S.A.* **99**, 15655–15660 (2002).
15. M. J. Wolf, G. M. Seleznik, N. Zeller, M. Heikenwalder, *Oncogene* **29**, 5006–5018 (2010).
16. J. Haybaeck *et al.*, *Cancer Cell* **16**, 295–308 (2009).
17. S. Jost, P. Turelli, B. Mangeat, U. Protzer, D. Trono, *J. Virol.* **81**, 10588–10596 (2007).
18. M. Lukashev *et al.*, *Cancer Res.* **66**, 9617–9624 (2006).
19. X. Hu *et al.*, *Carcinogenesis* **34**, 1105–1114 (2013).
20. E. Dejardin *et al.*, *Immunity* **17**, 525–535 (2002).
21. R. Suspène *et al.*, *Proc. Natl. Acad. Sci. U.S.A.* **102**, 8321–8326 (2005).
22. J. I. Friedman, J. T. Stivers, *Biochemistry* **49**, 4957–4967 (2010).
23. M. D. Stenglein, M. B. Burns, M. Li, J. Lengyel, R. S. Harris, *Nat. Struct. Mol. Biol.* **17**, 222–229 (2010).
24. M. Bonvin *et al.*, *Hepatology* **43**, 1364–1374 (2006).

25. T. Zhang *et al.*, *Hum. Mol. Genet.* **22**, 1262–1269 (2013).
26. Y. Huang *et al.*, *Gastroenterology* **132**, 733–744 (2007).
27. B. P. Doehle, A. Schäfer, B. R. Cullen, *Virology* **339**, 281–288 (2005).
28. G. Berger *et al.*, *PLOS Pathog.* **7**, e1002221 (2011).
29. H. Muckenfuss *et al.*, *J. Biol. Chem.* **281**, 22161–22172 (2006).
30. C. Münk, A. Willemsen, I. G. Bravo, *BMC Evol. Biol.* **12**, 71 (2012).
31. M. A. Carpenter *et al.*, *J. Biol. Chem.* **287**, 34801–34808 (2012).
32. P. Turelli, B. Mangeat, S. Jost, S. Vianin, D. Trono, *Science* **303**, 1829 (2004).
33. C. T. Bock *et al.*, *J. Mol. Biol.* **307**, 183–196 (2001).
34. M. M. Aynaud *et al.*, *J. Biol. Chem.* **287**, 39182–39192 (2012).
35. Y. Guo *et al.*, *BMC Genomics* **13**, 563 (2012).
36. H. C. Smith, R. P. Bennett, A. Kizilyer, W. M. McDougall, K. M. Prohaska, *Semin. Cell Dev. Biol.* **23**, 258–268 (2012).
37. T. H. Lee, S. J. Elledge, J. S. Butel, *J. Virol.* **69**, 1107–1114 (1995).
38. K. Kitamura *et al.*, *PLOS Pathog.* **9**, e1003361 (2013).
39. S. Landry, I. Narvaiza, D. C. Linfesty, M. D. Weitzman, *EMBO Rep.* **12**, 444–450 (2011).
40. M. B. Burns *et al.*, *Nature* **494**, 366–370 (2013).
41. K. Krebs *et al.*, *Gastroenterology* **145**, 456–465 (2013).

Acknowledgments: We thank R. Bester, T. Asen, K. Ackermann, K. Kappes, M. Feuerherd, R. Baier, R. Hillermann, U. Finkel, A. Krikoni, and F. Zhang for technical support; L. Terracciano for analysis of acute hepatitis patients; F. Chisari for HBV transgenic mice (HBV 1.3.32); T. Buch and O. Prazeres da Costa for help with array analysis and data discussions; L. Allweiss and A. Groth for help in generating and treating humanized uPA-SCID mice; and Siemens Healthcare Diagnostics for reagents. Supported by grants from Fédération Belge Contre le Cancer (E.D.), a European Research Council starting grant (LiverCancerMechanism) (M.H.), the German Research Foundation (SFB 841 to M.D., SFB TR 36 to M.H., and SFB TR 22), the Peter-Hans Hofschneider Foundation and the Helmholtz Alliances HAIT (U.P.), and PCCC (M.H.). We acknowledge the support of the nonprofit foundation HTCR, which holds human tissue on trust, making it broadly available for research on an ethical and legal basis. Patent application EP12006XXX has been filed at the European patent office: "Lymphotoxin signaling activation and its downstream mediators eliminate HBV ccc DNA." Microarray data have been submitted to the GEO database (www.ncbi.nlm.nih.gov/geo/) with accession number GSE46667. Human liver chimeric uPA-SCID mice were handled in accordance with protocols approved by the ethical committee of the city and state of Hamburg (permission number G12/015). Experiments with HBV-transgenic mice were performed in accordance with German legislation governing animal studies and the Principles of Laboratory Animal Care guidelines, NIH (55.1-1-54-2531.3-27-08). The study protocol for the animal experiment in fig. S12B was approved at the Southwest Foundation for Biomedical Research, San Antonio, TX (IACUC 869 PT, approved in 2004).

Supplementary Materials

www.sciencemag.org/content/343/6176/1221/suppl/DC1
Materials and Methods
Figs. S1 to S21
Table S1
References (*42*–*62*)

18 July 2013; accepted 5 February 2014
Published online 20 February 2014;
10.1126/science.1243462

REPORTS

Free-Standing Single-Atom-Thick Iron Membranes Suspended in Graphene Pores

Jiong Zhao,[1,3] Qingming Deng,[2] Alicja Bachmatiuk,[1,3,4] Gorantla Sandeep,[1] Alexey Popov,[2] Jürgen Eckert,[1,5] Mark H. Rümmeli[3,6]*

The excess of surface dangling bonds makes the formation of free-standing two-dimensional (2D) metals unstable and hence difficult to achieve. To date, only a few reports have demonstrated 2D metal formation over substrates. Here, we show a free-standing crystalline single-atom-thick layer of iron (Fe) using in situ low-voltage aberration-corrected transmission electron microscopy and supporting image simulations. First-principles calculations confirm enhanced magnetic properties for single-atom-thick 2D Fe membranes. This work could pave the way for new 2D structures to be formed in graphene membranes.

The success and promise of atomically thin carbon–namely, graphene (*1*)–has triggered enormous enthusiasm for the study of other two-dimensional (2D) materials such as hBN, MoS_2, and $MoSe_2$ (*2*, *3*). These 2D films are able to be reduced to atomically thin layers while still maintaining mechanical integrity, because they are layered structures where the bonding within a layer is covalent whereas the interlayer bonding occurs through weak van der Waals interactions, thus allowing individual layers to be easily separated. With bulk metals, at first glance, the nature of metallic bonding and their 3D structure prohibit them from existing as a monoatomic layer. The only reports for atomically thin metallic layers, thus far, are heteroepitaxial structures in which the metal atoms bond with the underlying substrates (*4*, *5*). On the other hand, because of nondirectional metallic bonding and the excellent plasticity of metals, at the nanoscale, one can build few-atom or even single-atom bridges (*6*, *7*). Many single atomic metallic layers (e.g., Fe, Co, and Mn) are attractive due to their inherent magnetic properties. For the case of 2D Fe monolayers, the magnetic moment is expected to be 3.1 μB, which is markedly higher than its bulk counterpart (2.2 μB), and, in addition, 2D Fe should have a large perpendicular magnetic anisotropy (*8*). Hence, 2D magnets could be promising for magnetic recording media. Most of what is known about 2D magnets is based on theoretical investigations. These studies point to their magnetic properties being highly sensitive to their structure (*9*). Face-centered cubic (FCC) Fe and body-centered cubic (BCC) Fe ultrathin films have been grown on Cu, W, SiC, MgO, and other surfaces (*9*–*13*). However, these structures interact with the underlying substrate. Free-standing 2D metal films do not suffer from substrate-based influences, thus preserving coordination and electron confinement.

Experimental and theoretical works have focused on the interactions between graphene and single metal atoms (including Fe atoms) (*14*–*16*) or clusters (*17*). We show that porous graphene under electron-beam irradiation can be extended to enable Fe atoms and clusters to entirely seal small perforations in graphene and form a single atomic crystalline Fe layer.

In our in situ investigation, a low-voltage spherical aberration-corrected transmission electron microscopy (LVACTEM) operating with an acceleration voltage of 80 kV was employed (*18*). The graphene samples were grown by chemical vapor deposition (CVD) over Ni/Mo substrates (*19*). The as-produced monolayer graphene was then transferred on to standard lacey carbon (TEM) grids using an $FeCl_3$ etching solution to detach the graphene (*20*). The transferred samples typically consist of large areas of monolayer graphene in which some regions contain remnant material from the transfer process, including remnant Fe species from decomposed $FeCl_3$ (*20*). Under close inspection, pure Fe can be found as small nanocrystals forming on the surface of the graphene, as single atoms or small clusters at the edge of pores in clean graphene, or as 2D crys-

[1]Leibniz-Institut für Festkörper- und Werkstoffforschung Dresden (IFW) Dresden, Institute of Complex Materials, P.O. Box 270116, D-01171 Dresden, Germany. [2]IFW Dresden, Institute of Solid State Research, P.O. Box 270116, D-01171 Dresden, Germany. [3]IBS Center for Integrated Nanostructure Physics, Institute for Basic Science (IBS), Daejon 305-701, Republic of Korea. [4]Centre of Polymer and Carbon Materials, Polish Academy of Sciences, M. Curie-Sklodowskiej 34, Zabrze 41-819, Poland. [5]Technische Universität Dresden, Institute of Materials Science, 01062 Dresden, Germany. [6]Department of Energy Science, Department of Physics, Sungkyunkwan University, Suwon 440-746, Republic of Korea.

*Corresponding author. E-mail: mark@rummeli.com

www.sciencemag.org/cgi/content/full/science.1243462/DC1

Supplementary Materials for

Specific and Nonhepatotoxic Degradation of Nuclear Hepatitis B Virus cccDNA

Julie Lucifora, Yuchen Xia, Florian Reisinger, Ke Zhang, Daniela Stadler, Xiaoming Cheng, Martin F. Sprinzl, Herwig Koppensteiner, Zuzanna Makowska, Tassilo Volz, Caroline Remouchamps, Wen-Min Chou, Wolfgang E. Thasler, Norbert Hüser, David Durantel, T. Jake Liang, Carsten Münk, Markus H. Heim, Jeffrey L. Browning, Emmanuel Dejardin, Maura Dandri, Michael Schindler, Mathias Heikenwalder,* Ulrike Protzer*

*Corresponding author. E-mail: protzer@tum.de (U.P.); heikenwaelder@helmholtz-muenchen.de (M.H.)

Published 20 February 2014 on *Science* Express
DOI: 10.1126/science.1243462

This PDF file includes:

Supplementary Materials

Materials and Methods

HBV inocula, cell cultures, HBV infection and treatments

HBV inolula were prepared as described (*42*) Shortly, HBV was concentrated from the supernatant of HepG2.2.15 cells using centrifugal filter devices (Centricon Plus-70, Biomax 100.000, Millipore Corp., Bedford, MA) and titered by HBV-DNA dot blot analysis after sedimentation into a CsCl density-gradient to determine enveloped DNA-containing viral particles (vp). Only inocula reaching a titer between $3x10^9$ and $3x10^{10}$ vp/mL were used. Immediately after collection, the virus stock was aliquoted and stored at -80°C until used for infection. Primary Human Hepatocytes (PHH) were isolated from surgical liver resections, cultured and infected with HBV as described (43, 44). Tissue samples and annotated data were obtained and experimental procedures were performed within the framework of the non profit foundation Human Tissue & Cell Research (HTCR), including the informed patient's consent (45). HepG2-H1.3, HepaRG and HepaRG-tA cell culture, differentiation and HBV infection (at a multiplicity of infection of 600 vp/cells) were also performed as described (13,46). HepaRG-tA-VifAU1 cell line was obtained after transduction of HepaRG-tA cells with a lentivirus expressing the HIV-Vif gene under tetracyclin regulated promoter (Plvx-Tight-Puro lentiviral vector, Clontech, Saint-Germain-en-Laye, France) and selection using 0.25 µg/ml puromycin. A3A or A3B overexpression in HepG2H1.3 cells was obtained by transfection of pLenti6.3, pLenti6.3-A3A, pTR600 or pTR600-A3B, respectively, using “Lipofectamine 2000 Reagent” (Invitrogen). No selection took place before experiment start. HepG2-H1.3-A3A cell line was obtained after lentiviral transduction of A3A into HepG2-H1.3 cells (47) and selection using 5ug/ml blasticidin. HepaRG cells were transfected with episomal replicon construct pEpi-H1.3 using “Lipofectamine® 2000 Reagent” (Invitrogen). pEpi-H1.3 was derived by cloning a 1.3-fold HBV genome into the extrachromosomal mammalian replicon plasmid pEpi-eGFP (kindly provided by H.J. Lipps, Witten-Herdecke, Germany). Two days after transfection, selection with 600 µg/ml geneticin was started and kept until cells expressed GFP and reached confluency and expressed GFP. HepaRG+pEpi-H1.3 cells were differentiated for 6 weeks to allow replication of HBV and establishment of HBV cccDNA by nuclear reimport of HBV rcDNA containing

capsids. Lamivudine and entecavir were used at 0.5 µM (5-fold and 1000-fold IC 50, respectively), IFN-α (Roferon-A, Roche) at 1000 U/mL and BS1, CBE11 and hu-IgG at 0.5 µg/mL unless otherwise indicated.

Analysis of HBV replication intermediates

HBeAg was determined using commercial immunoassays (Siemens Molecular Diagnostics, Marburg, for cell culture supernatants; Abbott Laboratories, Wiesbaden, Germany for mouse sera). Total DNA was purified from infected cells using a "Tissue kit" (Macherey Nagel, Düren, Germany). Total RNA was extracted from infected cells (NucleoSpin® RNA II kit, Macherey Nagel) and transcribed into cDNA using SuperScript III reverse transcriptase (Invitrogen). HBV-DNA, cccDNA and pgRNA were detected using specific PCR primers as described (48,17). pEpi-H1.3 was quantified using Kan-L/-R primers (see primer list). Real-time PCRs (qPCR) were performed using the LightCycler™ system (Roche Diagnostics) and analyzed using the second derivative maximum method that includes both normalization to the reference gene (*PrnP* for cccDNA and pEpi-H1.3 and GAPDH for pgRNA) and to primer efficiency (47,49). cccDNA specific primers span the gap and the nick in the rc form of the HBV genome and were designed not to detect rcDNA or a linear 1.1 or 1.3-fold HBV genome. Using optimized PCR conditions on the Light Cycler instrument (95°C for 10', 45 cycles at 95°C for 15'', 60°C for 5'', 72°C for 45'', and detection at 88°C for 2'' after each cycle), we determined the specificity to amplify cccDNA over rcDNA to be 10^3 to 1. For Southern Blot analyses, cccDNA was extracted from HBV-infected cells using the KCl protein precipitation method, separated through 0.8 % agarose gel, blotted onto nylon membrane and hybridized with ^{32}P HBV-DNA probe (50, 51). Quantification of cccDNA by qPCR was confirmed by quantification from Southern blotting as exemplarily shown in Figure S3B.

3D-PCR

PCR products from cccDNA-specific qPCR were diluted 1/20 to 1/50 and used as templates for nested PCR using HBxin fw and HBxin rev primers (see primer list) and decreasing denaturation temperatures as indicated. PCR products were purified by gel extraction (GeneJET Gel Extraction Kit, Fermentas, Fisher Scientific - Germany, Schwerte, Germany) and cloned by TA cloning (TA Cloning® Kit, Invitrogen). DNA from individual clones was purified (GeneJET

Plasmid Miniprep Kit, Fermentas, Fisher Scientific - Germany GmbH) and sequenced using primers hybridizing to the 5' and 3' plasmid backbone.

AP site quantification and repair

AP site quantification was performed with OxiSelect™ Oxidative DNA Damage Quantitation Kit (AP sites) (STA-324, Cell Biolabs, San Diego, CA, USA) according to the manufacturer's instruction using 0.5 µg of purified DNA (100 µg/mL). 1µg of total DNA were digested with 10 units of apurinic apyrimidinic endonuclease redox effector factor-1 (APE1; M0282L, New England Biolabs, Inc., Ipswich, MA, USA) or 1 µl PreCR Repair Mix (M0309L, New England Biolabs, Inc.).

qRT-PCR

For qRT-PCR RNA was extracted using commercial kits (RNeasy-kit from Qiagen, Hilden, Germany or NucleoSpin® RNA II kit, Macherey Nagel) and transcribed into cDNA with the Quantitect Reverse Transcription kit (Qiagen) or with SuperScript III reverse transcriptase (Invitrogen) according to the manufacturer's instructions. Expression levels were quantified by qRT-PCR performed on a 7900 HT qRT-PCR system (Applied Biosystems, Life Technologies Darmstadt, Germany) using the ΔΔCT method or on a LightCycler™ system (Roche Diagnostics) and analyzed using the second derivative maximum method that includes both normalization to the reference genes and primer efficiency. Relative mRNA levels of all target genes were normalized to at least two house-keeping genes (HPRT; RHOT2; TBP; GAPDH) levels.

siRNA and antibodies

siRNAs were obtained from Thermo Fisher Scientific Dharmacon® (Lafayette, CO, USA) : control siRNA (D-001910-10-05 Acell non-targeting pool 5nmol), siRNA against A3B (E-017322-00-0005, Accell SMARTpool, Human A3B (9582), 5 nmol) or siRNA against A3A (#E-017432-00, Accell SMARTpool). For Western blot analyses, immunostaining and immunoprecipitation, the following primary antibodies were used: polyclonal anti-NFkB2 p100/p52 (#4882, Cell Signaling Technology, Inc, Danvers, MA, USA), anti-phospho-RelA (#RB-1638-P0, Cell Signaling Technology), monoclonal anti-GAPDH (clone 14C10) (Cell

Signaling Technology), anti-β actin (clone 13E5) (Cell Signaling Technology), polyclonal anti-LTβR (#sc-8375,Santa Cruz Biotechnology, Inc, Heidelberg, Germany), anti-phospho-NIK (#4994, Santa Cruz Biotechnology), anti-TNFRI (#ab19139, Abcam, Cambridge, MA, USA), rabbit anti-HBVcore antiserum H800 (kindly provided by Heinz Schaller, Heidelberg, Germany), rabbit polyclonal anti-HBVcore (B0586, Dako, Hamburg, Germany), mouse monoclonal anti-HBVcore (F8.27.2, kindly provided by Dr. Marie-Anne Petit), anti-RelB (#sc-226, Santa Cruz Biotechnology), polyclonal anti–A3A (#AP31973PU-N, Acris Antibodies GmbH, Herford, Germany), polyclonal anti–A3F (#H00200316-A01; Abnova, Aachen, Germany), polyclonal anti–A3G (#AP23049PU-N, Acris Antibodies GmbH), polyclonal anti–AU1 (#A190-125A-2, Bethyl Laboratories, Inc., Montgomery, TX, USA), polyclonal anti-A3B (#sc-130955, Santa Cruz Biotechnology Inc), anti-Flag (F7425, Sigma), anti–TBP polyclonal antibody (H00006908-A01, Bethyl, USA), polyclonal anti–histone H3 (#ab1791, Abcam).

Deep sequencing

Target genes were amplified from total DNA by PCR using primers (see table below) designed to span around 2000bp of genomic sequence containing at least one exon and one intron. PCR reaction was performed with the Advantage®-HF2 PCR-kit (Clontech). Subsequently, amplicons were separated by a 0.8% agarose gel and purified using the S.N.A.P.™ UV-free gel purification kit (Life Technologies). Purified amplicons were submitted for deep sequencing to a commercial provider (GATC Biotech, Konstanz, Germany) and analyzed using Hiseq2000 sequencing system (Illumina, San Diego, CA, USA). Sequencing data were analyzed with CLC Genomics Workbench 6.01 (CLC bio, Aarhus, Denmark).

Nr.	Oligoname	Sequence (5'->3')
1	B2M fwd	CTGCCGTGTGAACCATGTGA
2	B2M rev	GCTACCTGTGGAGCAACCTG
3	CCL17 fwd	ACACAGAGACTCCCTCCTGG
4	CCL17 rev	GCTCCAGTTCAGACAAGGGG
5	CXCL10 fwd	AGCAGAGGAACCTCCAGTCT
6	CXCL10 rev	TGTGGTCCATCCTTGGAAGC
7	CXCL13 fwd	CGACATCTCTGCTTCTCATGC
8	CXCL13 rev	AGACTGAGCTCTCTTGGACAC
9	HMBS fwd	GGGCTCAGTGTCCTGGTTAC
10	HMBS rev	CCCAGAGCCCTCTAGACCTT

11	IL-6 fwd	GAGGAGACTTGCCTGGTGAAA
12	IL-6 rev	GCCCATGCTACATTTGCCG
13	MxA fwd	TCCATGACTCGCAGAGAGGA
14	MxA rev	TCCACTGTAGAACACGCCAC
15	MYC fwd	CCACCTCCAGCTTGTACCTG
16	MYC rev	GCTGCGTAGTTGTGCTGATG
17	PKR fwd	CTTGCCGTCACGGGGATAAT
18	PKR rev	CTTGGCATTAAGTCGCTGCC
19	PML fwd	GAAAGCCCAAAGCCAACAGG
20	PML rev	ATTGGCAGGATGGTTGAGGG
21	SRC fwd	TGGAACTTGCCAGGGTTGTT
22	SRC rev	ACCAGGGCAGGAAATGTAGC
23	TBP fwd	TTGGTAGTTGAATCCCGCCC
24	TBP rev	TCACTGTGAAGAGAGCGCAG

Immunofluorescence microscopy

Cells grown on 4-well-glass slide (Lab-Tek II, Fisher Scientific - Germany, Schwerte, Germany) were fixed with 4% paraformaldehyde (PFA) in PBS pH 7.4 for 10 min at room temperature and permeabilized with 0.5% saponin. Slides were blocked in PBS containing 0.5% saponin and 10% serum from the species that the secondary antibody was raised in at room temperature for two hours. After blocking, primary antibodies diluted in PBS with 0.1% saponin and 10% blocking serum were added overnight at 4°C. After extensive washing, slides were incubated with the secondary antibody in PBS with 0.1% saponin and 2% blocking serum for 2 hours at room temperature in the dark. Slides were mounted with Dapi Fluoromount-G (SouthernBiotech, Birmingham, Alabama, USA) and images were captured with a Olympus FV10i confocal Microscope (Olympus, Germany).

Expression profile analyses

Total RNA was amplified and labeled using WT Expression Kit (Ambion, Life Technologies) and Terminal labeling Kit (Affymetrix, Santa Clara, CA, USA) according to the manufacturer's recommendations. The amplified and fragmented, biotinylated complementary RNA was hybridized to Affymetrix Human Gene 1.0 ST Arrays (33297 probe sets) using standard procedures. The experimental setup contained a total of 8 arrays, made up of 2 groups, with each group consisting of 4 biological replicates. Arrays were assessed for quality and robust multi-array average (RMA)-normalized. Quality assessment consisted of RNA degradation plots,

Affymetrix quality control metrics, sample cross-correlation, and probe-level visualizations. Normalization included (separately for each RNA-type data set) background correction, quantile normalization, and probe-level summation by RMA. Data were analyzed for differential gene expression using an empirical Bayes moderated t-test (52), implemented in the Bioconductor package Linear Models for Microarray Data LIMMA. Results were sorted by the adjusted p-value and exported in tab-delimited format. Samples with an up- or downregulation ≥ 2 were re-analysed by qRT-PCR. Microarray data have been submitted to the GEO database (http://www.ncbi.nlm.nih.gov/geo/) and have the accession number GSE46667.

Immunoprecipitation assays

Co-Immunoprecipitations were performed using Pierce Co-Immunoprecipitation Kit (Fisher Scientific - Germany, Schwerte, Germany) according to the manufacturer's instructions. Chromatin immunoprecipitation was performed using Pierce Agarose ChIP Kit (#26156, Fisher Scientific) or ChIP kit #ab500 (Abcam, Cambridge, UK). Non-sheared DNA for cccDNA or MNase digested DNA for genomic DNA was analyzed by specific qPCR (GAPDH, P53, SRC, cMyc promoter regions).

FACS-based FRET

For FACS-FRET analysis we used a FACS CantoII Cytometer (BD Bioscience) with 405 nm, 488 nm and 633 nm lasers. Gating strategy and experimental procedures were done as described previously (*14*). eYFP was excited with 488 nm and detected with a 529/24 filter (Semrock, New York, USA) and eCFP was excited with 405 nm and detected via the 450/40 filter (Semrock). Huh7.5 hepatoma cells transfected with 1.6 µg DNA per 250.000 cells using Lipofectamine (Life technology) were used for FRET analysis. After 24 h, cells were washed, trypsinized and analyzed by flow cytometry using excitation at 405 nm followed by signal detection with the 529/24 filter. Mock transfected cells, eCFP and eYFP only as well as eCFP/eYFP co-transfected cells served as controls to exclude false positive FRET and subtract background signals. An eCFP-eYFP fusion construct was used as positive control. FRET constructs used within this study were all fused to eCFP/eYFP via their C-terminus using the *NheI-AgeI* restriction sites as previously described (53). PCR derived inserts were sequenced to confirm their identity.

Proximity ligation assay (PLA)

For PLA, cells were fixed with 1 % PFA, washed and permeabilized for 20 min with 1 % Saponin in PBS and blocked for 45 min with PLA blocking solution. Polyclonal rabbit anti-HBVcore and goat anti-A3A antibodies were incubated at a concentration of 1:100 in 1 % BSA for 2 h at RT. Secondary antibody probe incubation, ligation and amplification reactions were done according to the manufacturer's instructions (Duolink, Sigma Aldrich). Spinning disc microscopy with a Nikon Ti Eclipse microscope equipped with a Perkin Elmer UltraViewVox System (Yokogawa CSU-X1) was done for sample imaging. Images were analyzed with the Volocity 6.2 software package (Perkin Elmer) and the implemented automated spot counting was used to assess the number of spots per cropped cell. Statistical analysis was done with GraphPad Prism 5.0 and a one-way analysis of variances (ANOVA).

Modeling of HBc/A3A interaction

A three-dimensional structure of HBV core protein was generated by automatic modeling mode of SWISS-MODEL server (swissmodel.expasy.org) (54). The crystal structure of the human hepatitis B virus capsid (PDB code 1QGT, chains D) (55) was adapted as a template to perform the homology-modeling. In silico docking of A3A (PDB code 2M65) (56) and modeled HBVcore was carried out by using Hex protein docking server (http://hexserver.loria.fr/) (57). The result was displayed and analyzed by Rasmol 2.7.5 (58).

HBV-transgenic mice and tissue analysis

6 months old, male hepatitis B virus transgenic mice (C57BL/6, strain HBV1.3.32) (59) received murine lymphotoxin-receptor agonizing (ACH6) or isotype control antibodies intra-peritoneally (2 mg/kg, body weight) three times a week. Animals were maintained under specified pathogen-free conditions. Experiments were performed in accordance to the German legislation governing animal studies and the Principles of Laboratory Animal Care guidelines, NIH (55.1-1-54-2531.3-27-08). Mice were sacrificed at indicated time points and serum as well as liver tissues were obtained. Murine livers were fixed in phosphate buffered saline containing 4% PFA for 24 hours. Fixed liver specimens were embedded in paraffin and 2 µm sections were mounted on glass slides. Immuno-histochemical stainings were performed with cleaved caspase 3 (Cell Signaling), HBVcore (Diagnostic Biosystems, Pleasanton, CA, USA), RelA (NeoMarkers / Lab vision

corporation, Fremont, CA, USA) and RelB (Santa Cruz Biotechnology Inc.) specific antibodies employing an automated BOND-MAX™ platform (Leica Biosystems, Wetzlar, Germany). Positively stained cells were counted in five independent high-power fields and extrapolated to numbers per square millimeter tissue area. Fresh murine liver tissue were homogenized mechanically and lysed in buffer (Tris-HCL [10mM], NaCl [100mM], EDTA [5mM], Triton-X100 [5%]) containing protease inhibitor (Roche Diagnostics). Lysates (30 µg/ lane) were subjected to 15% SDS-PAGE (Bio-Rad, München, Germany) and blotted on nitrocellulose membranes (Bio-Rad) for Western blot analyses. Northern blot analyses were performed with total RNA isolated from cryopreserved liver tissue using TIRZOL® (Invitrogen).

Human chimeric uPA/SCID mice

Human liver-chimeric UPA/SCID mice were generated by transplanting one million thawed primary human hepatocytes and housed under specific pathogen-free conditions in accordance with protocols approved by the Ethical Committee of the city and state of Hamburg (permission number G12/015) (60). Levels of human chimerism were determined by measuring human serum albumin (HSA) in mouse serum (Human Albumin ELISA kit, Immunology Consultants Lab, Portland, USA) (61). HBV-infected mice received human lymphotoxin-receptor agonizing (CBE11) or isotype control antibodies intra-peritoneally (2mg/kg, body weight) once per week after macrophage depletion using clodronate liposomes (http://clodronateliposomes.org). Liver specimens collected at sacrifice were snap-frozen in 2-methylbutane for molecular analyses.

Chimpanzees

Remaining liver biopsies from a study performed on chimpanzees in 2004 were used (26). The study protocol was approved at the Southwest Foundation for Biomedical Research, San Antonio, TX (IACUC 869 PT, approved in 2004). Briefly, animals were treated with 10 million IU of recombinant human interferon-alpha2a and serial liver biopsies were performed at various time points to monitor induction of hepatic genes. Total RNA was extracted from chimpanzee liver biopsies with Trizol reagent (Life Science) and quantified using the NanoDrop spectrophotometer (NanoDrop Technologies). For each reverse transcription reaction, 360 ng of total RNA was converted into cDNA with Transcriptor First Strand cDNA Synthesis kit (Roche, Indianapolis, IN, USA) in 20 ul reaction volume. Taqman assay was used to assess the relative

level of the selected transcripts by normalizing to 18s RNA with the delta/delta Ct calculation method. Primers and probes were designed and synthesized by Integration DNA Technologies (Coraville, IA). All qPCR reactions were performed in a 10 µl volume and run on ABI VIIA 7 (Applied Biosystems, Foster City, CA, USA). Each reaction contained 5 µl 2X TaqMan universal PCR master mix (Applied Biosystems,), 0.5 uM of each primer, 0.25 uM of the probe, and cDNA (equivalent to ~16 ng total RNA). The amplification profile was initiated by 10 minute incubation at 95 °C, followed by two-step amplification of 15 seconds at 95 °C and 60 seconds at 60 °C for 40 cycles. For each treatment, results were expressed relative to the expression of the pre-treated chimpanzee liver biopsies as fold-induction. Forward and reverse primers and probes for the selected genes were designed and are listed in Table 1.

GENES	Ref Seq	PROBES(5'-3')	FORWARD PRIMER(5'-3')	REVERSE PRIMER(5'-3')
APOBEC3A	NM_001270406.1	/56-FAM/TGC AGT AGC /ZEN/ GCA ATC TCG GCT C/3IABkFQ/	AGA TGG AGT CTG GTA CTG TCG	GAG GCA GGA GAG TAG CGT
APOBEC3B	NM_004900.4	/56-FAM/CCA CAG ATC /ZEN/ AGA AAT CCG ATG GAG CG/3IABkFQ/	GAC AGG GAC AAG CGT ATC TAA G	TCA CTT CAT AGC ACA GCC AAG
APOBEC3C	NM_014508	/56-FAM/AAC CCG ATG /ZEN/ AAG GCA ATG TAT CCA GG/3IABkFQ/	CAG AAA AGA GTG GGA CAG GG	ACA GCC AAG TTT CGT TCC G
APOBEC3D	M_152426	/56-FAM/CCA CAG ATC /ZEN/ AGA AAT CCG ATG GAG CG/3IABkFQ/	GAC TGG GAC AAG CGT ATC TAA G	TCA CTT CAT AGC ACA GCC AAG
APOBEC3F	NM_145298	/56-FAM/TGG GAA TAC /ZEN/ACC TGG CCT CGA AAG /3IABkFQ/	CGA AGT GAA AAC AAA GGG TCC	GGA AAC ACT TGT AAG CAG GC
APOBEC3G	NM_021822.3	/56-FAM/CGG AAT ACA /ZEN/CCT GGC CTC GAA AGA T/3IABkFQ/	CGA AGT GAA AAC AAA GGG TCC	CAT ACT CCT GGT CAC GAT GC
APOBEC3H	NM_001166003	/56-FAM/ACG GGT CCA /ZEN/AGC TGC AAA CTT CT/3IABkFQ/	CGA CGG CTT GAG AGG ATA AAG	GGC TAT GAG GCA ACT GAC ATG
TBP	NM_003194	/56-FAM/TGG GAT TAT /ZEN/ATT CGG CGT TTC GGG C/3IABkFQ/	GAG AGT TCT GGG ATT GTA CCG	ATC CTC ATG ATT ACC GCA GC

Analyses of HCV-infected patients treated with PEG-IFN-α

To investigate the effect of IFN-α treatment on APOBEC RNA expression in the human liver we used previously published microarray data of paired liver biopsies from HCV-infected patients undergoing antiviral therapy (62) (Michael T. Dill, Zuzanna Makowska, Gaia Trincucci, Andreas J. Gruber, Julia E. Vogt, Magdalena Filipowicz, Diego Calabrese, Ilona Krol, Daryl T. Lau,

Luigi Terracciano, Erik van Nimwegen, Volker Roth, and Markus H. Heim. Pegylated interferon-α regulates hepatic gene expression by transient activation of the Jak-STAT pathway. Journal of Clinical Investigation, in press). This study included 18 HCV patients who all had a liver biopsy performed during the diagnostic workup and a second liver biopsy collected 4h, 16h, 48h, 96h, or 144h after the first injection of 1.5 ug/kg body weight pegIFNalpha-2b (PegIntron™, MSD). The patients were subsequently treated with standard combination therapy of pegIFNalpha-2b and ribavirin.

Primers list

Nr.	Oligoname	Sequence (5'->3')
1	ABCA12 fwd	TCTTTTCTTCGCAATGGTTCCT
2	ABCA12 rev	GCTGGCATGACTTCTCTATCAAA
3	ABCB4 fwd	ATAGCTCACGGATCAGGTCTC
4	ABCB4 rev	GGATTTAGCAGCGACAAGGAAA
5	ADAMTS9 fwd	ATTAGAGACCCTGAGCGAATACG
6	ADAMTS9 rev	GAAGTGGACGTTCGTGGGAA
7	ADH1C fwd	GTTGCACCTCCTAAGGCTCAT
8	ADH1C rev	GTTGCCACTAACCACATGCT
9	AICDA fwd	GACTTTGGTTATCTTCGCAATAAGA
10	AICDA rev	AGGTCCCAGTCCGAGATGTA
11	AKR1B10 fwd	GTGACACCAGCACGCATTG
12	AKR1B10 rev	GCATTGAAGGGATAGTCTTCCAA
13	ALDOB fwd	GGCAGTTCCGAGAAATCCTCT
14	ALDOB rev	CTCCTTGGTCTAACTTGATTCCC
15	ANKH fwd	TCGTGGTCCTACCCTACCTG
16	ANKH rev	TGGATTCTCCCACAAAGCCC
17	ANLN fwd	ATCTTGCTGCAACTATTTGCTCC
18	ANLN rev	TCCTGCTTAACACTGCTGCTA
19	AOX1 fwd	TGTCGATCCTGAAACAATGCTG
20	AOX1 rev	GGTGATGGGGTTGTATCGTGA
21	APOBEC3A fwd	GAGAAGGGACAAGCACATGG
22	APOBEC3A rev	TGGATCCATCAAGTGTCTGG
23	APOBEC3B fwd	GACCCTTTGGTCCTTCGAC
24	APOBEC3B rev	GCACAGCCCCAGGAGAAG
25	APOBEC3C fwd	AGCGCTTCAGAAAAGAGTGG
26	APOBEC3C rev	AAGTTTCGTTCCGATCGTTG
27	APOBEC3DE fwd	CACATTTCTGCGTGGTTCTC
28	APOBEC3DE rev	ACCCAAACGTCAGTCGAATC
29	APOBEC3F fwd	CCGTTTGGACGCAAAGAT

30	APOBEC3F rev	CCAGGTGATCTGGAAACACTT
31	APOBEC3G fwd	CCGAGGACCCGAAGGTTAC
32	APOBEC3G rev	TCCAACAGTGCTGAAATTCG
33	APOBEC3H fwd	AGCTGTGGCCAGAAGCAC
34	APOBEC3H rev	CGGAATGTTTCGGCTGTT
35	APOBEC4 fwd	TTCTAACACCTGGAATGTGATCC
36	APOBEC4 rev	TTTACTGTCTTCTAGCTGCAAACC
37	APOC3 fwd	TCAGACCAACTTCAGCCGTG
38	APOC3 rev	GAGCTCGCAGGATGGATAGG
39	ARNT2 fwd	CGTCACCCCTGTTCTGAACC
40	ARNT2 rev	CGGCCTGTCATTGAGTTTTCT
41	ASF1B fwd	TCATCCGAGTGGGCTACTACG
42	ASF1B rev	GTTGTTGTCCCAGTTGATATGGA
43	BID fwd	GTAGTCGACCGTGTCCGC
44	BID rev	AACCGTTGTTGACCACCCTC
45	BIRC3 fwd	TTTCCGTGGCTCTTATTCAAACT
46	BIRC3 rev	GCACAGTGGTAGGAACTTCTCAT
47	C4B fwd	TCCAGGACCTCTCTCCAGTG
48	C4B rev	CCCCCAAAAATGAGCTTGCC
49	C5MTF fwd	GGAAATTAGAATCAAGGAAATACGA
50	C5MTF fwd	AATTTGTCTTGAGGCGCTTG
51	C6 fwd	TTGATGGGCAATGGGTTTCAT
52	C6 rev	ACTTGTCCTACTGCTTTTGACAG
53	cccDNA 2251 rev	AGCTGAGGCGGTATCTA
54	cccDNA 92 fwd	GCCTATTGATTGGAAAGTATGT
55	CCL5 fwd	TCACGCCATTCTCCTG
56	CCL5 rev	CCCCTCACTATCCTACC
57	CCNA2 fwd	GGATGGTAGTTTTGAGTCACCAC
58	CCNA2 rev	CACGAGGATAGCTCTCATACTGT
59	CD44 fwd	GCATCGGATTTGAGACCTGC
60	CD44 rev	CTGAGACTTGCTGGCCTCTC
61	CD74 fwd	CCGGCTGGACAAACTGACA
62	CD74 rev	GGTGCATCACATGGTCCTCTG
63	CDC20 fwd	GCACAGTTCGCGTTCGAGA
64	CDC20 rev	CTGGATTTGCCAGGAGTTCGG
65	CKAP2 fwd	GTCCATCAGCATTAAACTCCAGC
66	CKAP2 rev	GTCAGCCTTTTGCCCAGAAGT
67	CKS2 fwd	CACTACGAGTACCGGCATGT
68	CKS2 rev	CACCAAGTCTCCTCCACTCC
69	cMyc-fwd	TCGAGAAGGGCAGGGCTTCTCAGAGGCTTG
70	cMyc-rev	GGCGATATGCGGTCCCTACTCCAAGGAGCT
71	CREB3L3 fwd	ATGAATACGGATTTAGCTGCTGG

72	CREB3L3 rev	AGGAAGTCGTCAGAGTCGGG
73	CTSE fwd	AGGCATCCGTCCCTCAAGAA
74	CTSE rev	CCTTGGCACTCTGGTCCATTG
75	CX3CL1 fwd	ACCACGGTGTGACGAAATG
76	CX3CL1 rev	TGTTGATAGTGGATGAGCAAAGC
77	CYP2B6 fwd	GCACTCCTCACAGGACTCTTG
78	CYP2B6 rev	CCCAGGTGTACCGTGAAGAC
79	CYP3A4 fwd	TTTTTGGATCCATTCTTTCTCTCAA
80	CYP3A4 rev	TCCACTCGGTGCTTTTGTGT
81	CYP4B1 fwd	CCCACTCTGGTTCGGACAG
82	CYP4B1 rev	ATACACATCAGGGGCCTTAGG
83	CYP4F3 fwd	CCCCGAAACGGAATTGGTTCT
84	CYP4F3 rev	TGTGTGTATAGGAGACCTTCCTC
85	CYP7A1 fwd	GAGAAGGCAAACGGGTGAAC
86	CYP7A1 rev	GGATTGGCACCAAATTGCAGA
87	DCLK1 fwd	GCTGATTTGACCCGAACTCTG
88	DCLK1 rev	AGCCACATACATAACTCTCTCCT
89	DIO1 fwd	GTCGTGGGTAAAGTGCTTCTG
90	DIO1 rev	GTTCCGCTTGACTCTGTCTGG
91	DTL fwd	TCACTGGAATGCCGTCTTTGA
92	DTL rev	CTCACCAGCTTTTACGTCCC
93	ECHDC2 fwd	CGACGACTGAGTGGAACTGAG
94	ECHDC2 rev	CCACAGCGTGATTCACCAG
95	EHHADH fwd	AAACTCAGACCCGGTTGAAGA
96	EHHADH rev	TTGCAGAGTCTACGGGATTCT
97	ETNK2 fwd	GCCCCGGCTTTTCAGGTTAAT
98	ETNK2 rev	GGCTGGGGTTGATCTCGTT
99	F13B fwd	TCAACCAACCTGTAGGAAAGAAC
100	F13B rev	AGCCAGTAGCACATTCGTATTG
101	G6PC fwd	CCCAGGTTCACCAGTTCCC
102	G6PC rev	GCCGTCATTATGGGCCAGA
103	GAPDH fwd	ACCAACTGCTTAGCCC
104	GAPDH rev	CCACGACGGACACATT
105	GNMT fwd	CTGGGGTGGACTCCATTATGC
106	GNMT rev	GATGACCCACTTGTCGAAGGC
107	GYPC fwd	GTGGCCTCTCAGCCTCG
108	GYPC rev	GGCTCTGCAATGGTGGTAGT
109	HAO2 fwd	GCATCACGCGGGATGACAA
110	HAO2 rev	GCGATACAAATAGGGGCACTGA
111	HBxin fwd	ATGGCTGCTARGCTGTGCTGCCAA
112	HBxin rev	AAGTGCACACGGTYYGGCAGAT
113	HIST13A fwd	ACTGCTCGGAAGTCTACTGGT

114	HIST13A rev	GCGCTGGAAAGGTAGTTTACGA
115	HJURP fwd	CCACGCTGACCTACGAGAC
116	HJURP rev	CTCACCGCTTTTTGAATCGGC
117	HRG fwd	GACGGGATGGCTACCTTTTCC
118	HRG rev	CCGATTCTTGCACATCTAAGACT
119	HSD11B1 fwd	AGCAGGAAAGCTCATGGGAG
120	HSD11B1 rev	CCACGTAACTGAGGAAGTTGAC
121	IFNGR2 fwd	ACTGGCTCCCTGGAAGAGAT
122	IFNGR2 rev	TGCAGGGACAGGCCTTTTAG
123	IKZF3 fwd	AAAGTGCAGCGGTTTTGAATG
124	IKZF3 rev	AGCTGTAAGGGATTTCAGGCT
125	ITGA3 fwd	CCCTGGCAGACCTGAACAAT
126	ITGA3 rev	AGACATAGATGGCACCCCCT
127	ITGAV fwd	ATCTGTGAGGTCGAAACAGGA
128	ITGAV rev	TGGAGCATACTCAACAGTCTTTG
129	Kan-L	GGCAGGATCTCCTGTCATCT
130	Kan-R	CATCAGCCATGATGGATACTTTC
131	KIF20A fwd	ACCTGATCTGAAGCCCTTGC
132	KIF20A rev	TGGTGCTGGTACCTATCCGA
133	LCN2 fwd	GAAGTGTGACTACTGGATCAGGA
134	LCN2 rev	ACCACTCGGACGAGGTAACT
135	LIPG fwd	GATGGACGATGAGCGGTATCT
136	LIPG rev	CGCATCCGTGTAAAGCTGG
137	MBD4 fwd	GGCAACGACTCTTACCGAAT
138	MBD4 rev	CCCAAAGCCAGTCATGATATTT
139	MKI67 fwd	TTCGCAAGCGCATAACCCA
140	MKI67 rev	AACCGTGTCACAGTGCCAAA
141	MTTP fwd	ACAAGCTCACGTACTCCACTG
142	MTTP rev	TCCTCCATAGTAAGGCCACATC
143	MxA fwd	GGTGGTCCCCAGTAATGTGG
144	MxA rev	CGTCAAGATTCCGATGGTCCT
145	NEIL3 fwd	TCTCCTGTTTTGGAAGTGCA
146	NEIL3 rev	CATTAGCACATCACCTAGCATCC
147	NFE2L3 fwd	TTCAGCCAGGCTATAAGTCAGG
148	NFE2L3 rev	GCTCAGGATTGGTGGTATGAGA
149	NFKB2 fwd	GGGCCGAAAGACCTATCCC
150	NFKB2 rev	CAGCTCCGAGCATTGCTTG
151	NFKBIE fwd	GGTCCACCTGGCAGTGATTC
152	NFKBIE rev	ACCATGCCGGTCCTGTAGT
153	NR0B2 fwd	CCCCAAGGAATATGCCTGCC
154	NR0B2 rev	TAGGGCGAAAGAAGAGGTCCC
155	NR1D1 fwd	TGGACTCCAACAACAACACAG

156	NR1D1 rev	GATGGTGGGAAGTAGGTGGG
157	NR1I3 fwd	TGGGCACCATGTTTGAACAGT
158	NR1I3 rev	GGGCAGGTCCTTAGTAAACTTG
159	OAS1 fwd	TGTCCAAGGTGGTAAAGGGTG
160	OAS1 rev	CCGGCGATTTAACTGATCCTG
161	PFKFB1 fwd	AGAAGGGGCTCATCCATACCC
162	PFKFB1 rev	CTCTCGTCGATACTGGCCTAA
163	pgRNA 383 fwd	CTCCTCCAGCTTATAGACC
164	pgRNA 705 rev	GTGAGTGGGCCTACAAA
165	PIPOX fwd	GCAGAGGGTAGAACACCAGTG
166	PIPOX rev	CCTAGCTGTCGAATTGCATCC
167	PKR fwd	GCCGCTAAACTTGCATATCTTCA
168	PKR rev	TCACACGTAGTAGCAAAAGAACC
169	PLA2G2A fwd	ATGAAGACCCTCCTACTGTTGG
170	PLA2G2A rev	GCTTCCTTTCCTGTCGTCAACT
171	PLK1 fwd	CGAGGACAACGACTTCGTGTT
172	PLK1 rev	ACAATTTGCCGTAGGTAGTATCG
173	PNPLA3 fwd	GGCATCTCTCTTACCAGAGTGT
174	PNPLA3 rev	GGCATCCACGACTTCGTCTTT
175	POR fwd	GGTGGCCGAAGAAGTATCTCT
176	POR rev	AACCAGTAGGTTAGGAGACCC
177	Prnp fwd	TGCTGGGAAGTGCCATGAG
178	Prnp rev	CGGTGCATGTTTTCACGATAGTA
179	PSMB9 fwd	GGTTCTGATTCCCGAGTGTCT
180	PSMB9 rev	CAGCCAAAACAAGTGGAGGTT
181	p53-fwd	GAGTGCAGTGGCACGATTT
182	p53-rev	GAATCGCTTTCAGCTCAGGA
183	RAC2fwd	CAACGCCTTTCCCGGAGAG
184	RAC2rev	TCCGTCTGTGGATAGGAGAGC
185	rcDNA1745 fwd	GTTGCCCGTTTGTCCTCTAATTC
186	rcDNA1844 rev	GGAGGGATACATAGAGGTTCCTTGA
187	RCN1 fwd	TGGATCAAACGGGTGCAGAA
188	RCN1 rev	TGCGGGGTTTCCTAGGTAGT
189	RDH5 fwd	TGGGTGGAGATGCACGTTAAG
190	RDH5 rev	GTGTGGGTCCGATGATACCAG
191	RRM2 fwd	ATTGGGCCTTGCGATGGATAG
192	RRM2 rev	GAGTCCTGGCATAAGACCTCT
193	SCP2 fwd	TACCCTGACTTGGCAGAAGAA
194	SCP2 rev	CTGGCGGGCCATAAACAAA
195	SERPINA7 fwd	TCACCATTCCTGTATCTGGTTCT
196	SERPINA7 rev	GTGGCATTTGGTTGGGATGAA
197	SERPIND1 fwd	GGACGACGACTATCTGGACCT

198	SERPIND1 rev	CATCAGAGTCTGTCGGGGAAA
199	SERPING1 fwd	CCAAGATGCTATTCGTTGAACCC
200	SERPING1 rev	TGGTGGCTGAATTGGTTGTTG
201	SLC17A4 fwd	ATGTCTACCGGACCAGATGTC
202	SLC17A4 rev	GCCCATGTCGGACTGAACAAA
203	SLC22A1 fwd	TGCCCCTCATTTTGTTTGCG
204	SLC22A1 rev	TTTCTCCCAAGGTTCTCGGC
205	SLC9A9 fwd	CAGCACAACATCAATCCTCATCA
206	SLC9A9 rev	CAGCATGTATCATAGCCTTCACA
207	SMUG1 fwd	CTGCAGTGCCTGTCATGTG
208	SMUG1 rev	GCAGGCTCATGGATGGAC
209	SOD2 fwd	GGAAGCCATCAAACGTGACTT
210	SOD2 rev	CCCGTTCCTTATTGAAACCAAGC
211	SPP1 fwd	CTCCATTGACTCGAACGACTC
212	SPP1 rev	CAGGTCTGCGAAACTTCTTAGAT
213	Src-fw	TGTGTGTGTGAGAAAACACAAAAT
214	Src-rev	TCAGTCCTCCCAGGATGTTC
215	SULT2A1 fwd	AGCGATCACCCTGGGTAGAG
216	SULT2A1 rev	TGGGAGGAGAATAAACGTGGAC
217	TAP1fwd	CGCCTCACTGACTGGATTCTA
218	TAP1rev	TCTGTTGGAAAAACTCCGTCTC
219	TAT fwd	CTGGACTCGGGCAAATATAATGG
220	TAT rev	GTCCTTAGCTTCTAGGGGTGC
221	TDG fwd	GAACCTTGTGGCTTCTCTTCA
222	TDG rev	GTCATCCACTGCCCATTAGG
223	TF fwd	GTGTGCAGTGTCGGAGCAT
224	Tf rev	CATCGGATGGAATGACGCTTT
225	TMEM123 fwd	GGCGGCATCTGCAAACATAG
226	TMEM123 rev	TTCATGGTGGTGACCGTTGT
227	TMPRSS2 fwd	CAAGTGCTCCAACTCTGGGAT
228	TMPRSS2 rev	AACACACCGATTCTCGTCCTC
229	TNFAIP3 fwd	TCAACTGGTGTCGAGAAGTCC
230	TNFAIP3 rev	CAAGTCTGTGTCCTGAACGC
231	TNFRSF9 fwd	TCCACCAGCAATGCAGAGTG
232	TNFRSF9 rev	CCAAAGCAACAGTCTTTACAACC
233	TOP2A fwd	ACCATTGCAGCCTGTAAATGA
234	TOP2A rev	GGGCGGAGCAAAATATGTTCC
235	TPX2 fwd	ACTTCCGCACAGATGAGCG
236	TPX2 rev	GGATGCTTTCGTAGTTCAGATGT
237	TRAF1 fwd	CGCCGAGATGGAGTCATCAG
238	TRAF1 rev	TGGAAATCCCCAGGGTGTTG
239	TYMS fwd	CTGCTGACAACCAAACGTGTG

240	TYMS rev	GCATCCCAGATTTTCACTCCCTT
241	UBD fwd	CCGTTCCGAGGAATGGGATTT
242	UBD rev	GCCATAAGATGAGAGGCTTCTCC
244	UGT2B10 fwd	GAAATGGACTACAGTTCTGCTGA
245	UGT2B10 rev	GTGGATGAGTCGTTGGGATCA
246	UGT2B4 fwd	CAAATGTTGAGTTCGTTGGAGGA
247	UGT2B4 rev	CTGACGTGTTACTGACCATCG
248	V-MYC fwd	GGCTCCTGGCAAAAGGTCA
249	V-MYC rev	CTGCGTAGTTGTGCTGATGT
250	VTN fwd	CGGGGATGTGTTCACTATGCC
251	VTN rev	GTGTCTGCTCAGGATTCCCTT

qRT-PCR primer sequences were either taken from the Harvard primer bank or newly established by using NCBI primer blast. All primer pairs were designed to span at least one intron/exon border to exclude genomic DNA amplification and checked for sequence specificity to avoid unspecific by-products. Correct amplicon size was checked by agarose gel-electrophoreses and melting curve analyses were done for each qPCR run.

References

1. U. Protzer, M. K. Maini, P. A. Knolle, Living in the liver: hepatic infections. *Nat. Rev. Immunol.* **12**, 201–213 (2012). doi:10.1038/nri3169 Medline

2. F. Zoulim, Hepatitis B virus resistance to antiviral drugs: where are we going? *Liver Int.* **31**, (Suppl 1), 111–116 (2011). doi:10.1111/j.1478-3231.2010.02399.x Medline

3. K. Wursthorn, M. Lutgehetmann, M. Dandri, T. Volz, P. Buggisch, B. Zollner, T. Longerich, P. Schirmacher, F. Metzler, M. Zankel, C. Fischer, G. Currie, C. Brosgart, J. Petersen, Peginterferon alpha-2b plus adefovir induce strong cccDNA decline and HBsAg reduction in patients with chronic hepatitis B. *Hepatology* **44**, 675–684 (2006). doi:10.1002/hep.21282 Medline

4. L. G. Guidotti, K. Ando, M. V. Hobbs, T. Ishikawa, L. Runkel, R. D. Schreiber, F. V. Chisari, Cytotoxic T lymphocytes inhibit hepatitis B virus gene expression by a noncytolytic mechanism in transgenic mice. *Proc. Natl. Acad. Sci. U.S.A.* **91**, 3764–3768 (1994). doi:10.1073/pnas.91.9.3764 Medline

5. L. G. Guidotti, R. Rochford, J. Chung, M. Shapiro, R. Purcell, F. V. Chisari, Viral clearance without destruction of infected cells during acute HBV infection. *Science* **284**, 825–829 (1999). doi:10.1126/science.284.5415.825 Medline

6. S. F. Wieland, H. C. Spangenberg, R. Thimme, R. H. Purcell, F. V. Chisari, Expansion and contraction of the hepatitis B virus transcriptional template in infected chimpanzees. *Proc. Natl. Acad. Sci. U.S.A.* **101**, 2129–2134 (2004). doi:10.1073/pnas.0308478100 Medline

7. H. McClary, R. Koch, F. V. Chisari, L. G. Guidotti, Relative sensitivity of hepatitis B virus and other hepatotropic viruses to the antiviral effects of cytokines. *J. Virol.* **74**, 2255–2264 (2000). doi:10.1128/JVI.74.5.2255-2264.2000 Medline

8. L. Belloni, L. Allweiss, F. Guerrieri, N. Pediconi, T. Volz, T. Pollicino, J. Petersen, G. Raimondo, M. Dandri, M. Levrero, IFN-α inhibits HBV transcription and replication in cell culture and in humanized mice by targeting the epigenetic regulation of the nuclear cccDNA minichromosome. *J. Clin. Invest.* **122**, 529–537 (2012). doi:10.1172/JCI58847 Medline

9. A. Rang, S. Günther, H. Will, Effect of interferon alpha on hepatitis B virus replication and gene expression in transiently transfected human hepatoma cells. *J. Hepatol.* **31**, 791–799 (1999). doi:10.1016/S0168-8278(99)80279-7 Medline

10. V. Pasquetto, S. F. Wieland, S. L. Uprichard, M. Tripodi, F. V. Chisari, Cytokine-sensitive replication of hepatitis B virus in immortalized mouse hepatocyte cultures. *J. Virol.* **76**, 5646–5653 (2002). doi:10.1128/JVI.76.11.5646-5653.2002 Medline

11. S. F. Wieland, L. G. Guidotti, F. V. Chisari, Intrahepatic induction of alpha/beta interferon eliminates viral RNA-containing capsids in hepatitis B virus transgenic mice. *J. Virol.* **74**, 4165–4173 (2000). doi:10.1128/JVI.74.9.4165-4173.2000 Medline

12. S. L. Uprichard, S. F. Wieland, A. Althage, F. V. Chisari, Transcriptional and posttranscriptional control of hepatitis B virus gene expression. *Proc. Natl. Acad. Sci. U.S.A.* **100**, 1310–1315 (2003). doi:10.1073/pnas.252773599 Medline

13. P. Gripon, C. Diot, N. Thézé, I. Fourel, O. Loreal, C. Brechot, C. Guguen-Guillouzo, Hepatitis B virus infection of adult human hepatocytes cultured in the presence of dimethyl sulfoxide. *J. Virol.* **62**, 4136–4143 (1988). Medline

14. P. Gripon, S. Rumin, S. Urban, J. Le Seyec, D. Glaise, I. Cannie, C. Guyomard, J. Lucas, C. Trepo, C. Guguen-Guillouzo, Infection of a human hepatoma cell line by hepatitis B virus. *Proc. Natl. Acad. Sci. U.S.A.* **99**, 15655–15660 (2002). doi:10.1073/pnas.232137699 Medline

15. M. J. Wolf, G. M. Seleznik, N. Zeller, M. Heikenwalder, The unexpected role of lymphotoxin beta receptor signaling in carcinogenesis: from lymphoid tissue formation to liver and prostate cancer development. *Oncogene* **29**, 5006–5018 (2010). doi:10.1038/onc.2010.260 Medline

16. J. Haybaeck, N. Zeller, M. J. Wolf, A. Weber, U. Wagner, M. O. Kurrer, J. Bremer, G. Iezzi, R. Graf, P. A. Clavien, R. Thimme, H. Blum, S. A. Nedospasov, K. Zatloukal, M. Ramzan, S. Ciesek, T. Pietschmann, P. N. Marche, M. Karin, M. Kopf, J. L. Browning, A. Aguzzi, M. Heikenwalder, A lymphotoxin-driven pathway to hepatocellular carcinoma. *Cancer Cell* **16**, 295–308 (2009). doi:10.1016/j.ccr.2009.08.021 Medline

17. S. Jost, P. Turelli, B. Mangeat, U. Protzer, D. Trono, Induction of antiviral cytidine deaminases does not explain the inhibition of hepatitis B virus replication by interferons. *J. Virol.* **81**, 10588–10596 (2007). doi:10.1128/JVI.02489-06 Medline

18. M. Lukashev, D. LePage, C. Wilson, V. Bailly, E. Garber, A. Lukashin, A. Ngam-ek, W. Zeng, N. Allaire, S. Perrin, X. Xu, K. Szeliga, K. Wortham, R. Kelly, C. Bottiglio, J. Ding, L. Griffith, G. Heaney, E. Silverio, W. Yang, M. Jarpe, S. Fawell, M. Reff, A. Carmillo, K. Miatkowski, J. Amatucci, T. Crowell, H. Prentice, W. Meier, S. M. Violette, F. Mackay, D. Yang, R. Hoffman, J. L. Browning, Targeting the lymphotoxin-beta receptor with agonist antibodies as a potential cancer therapy. *Cancer Res.* **66**, 9617–9624 (2006). doi:10.1158/0008-5472.CAN-06-0217 Medline

19. X. Hu, M. A. Zimmerman, K. Bardhan, D. Yang, J. L. Waller, G. B. Liles, J. R. Lee, R. Pollock, D. Lev, C. F. Ware, E. Garber, V. Bailly, J. L. Browning, K. Liu, Lymphotoxin β receptor mediates caspase-dependent tumor cell apoptosis in vitro and tumor suppression in vivo despite induction of NF-κB activation. *Carcinogenesis* **34**, 1105–1114 (2013). doi:10.1093/carcin/bgt014 Medline

20. E. Dejardin, N. M. Droin, M. Delhase, E. Haas, Y. Cao, C. Makris, Z. W. Li, M. Karin, C. F. Ware, D. R. Green, The lymphotoxin-beta receptor induces different patterns of gene expression via two NF-kappaB pathways. *Immunity* **17**, 525–535 (2002). doi:10.1016/S1074-7613(02)00423-5 Medline

21. R. Suspène, D. Guétard, M. Henry, P. Sommer, S. Wain-Hobson, J. P. Vartanian, Extensive editing of both hepatitis B virus DNA strands by APOBEC3 cytidine deaminases in vitro and in vivo. *Proc. Natl. Acad. Sci. U.S.A.* **102**, 8321–8326 (2005). doi:10.1073/pnas.0408223102 Medline

22. J. I. Friedman, J. T. Stivers, Detection of damaged DNA bases by DNA glycosylase enzymes. *Biochemistry* **49**, 4957–4967 (2010). doi:10.1021/bi100593a Medline

23. M. D. Stenglein, M. B. Burns, M. Li, J. Lengyel, R. S. Harris, APOBEC3 proteins mediate the clearance of foreign DNA from human cells. *Nat. Struct. Mol. Biol.* **17**, 222–229 (2010). doi:10.1038/nsmb.1744 Medline

24. M. Bonvin, F. Achermann, I. Greeve, D. Stroka, A. Keogh, D. Inderbitzin, D. Candinas, P. Sommer, S. Wain-Hobson, J. P. Vartanian, J. Greeve, Interferon-inducible expression of APOBEC3 editing enzymes in human hepatocytes and inhibition of hepatitis B virus replication. *Hepatology* **43**, 1364–1374 (2006). doi:10.1002/hep.21187 Medline

25. T. Zhang, J. Cai, J. Chang, D. Yu, C. Wu, T. Yan, K. Zhai, X. Bi, H. Zhao, J. Xu, W. Tan, C. Qu, D. Lin, Evidence of associations of APOBEC3B gene deletion with susceptibility to persistent HBV infection and hepatocellular carcinoma. *Hum. Mol. Genet.* **22**, 1262–1269 (2013). doi:10.1093/hmg/dds513 Medline

26. Y. Huang, J. J. Feld, R. K. Sapp, S. Nanda, J. H. Lin, L. M. Blatt, M. W. Fried, K. Murthy, T. J. Liang, Defective hepatic response to interferon and activation of suppressor of cytokine signaling 3 in chronic hepatitis C. *Gastroenterology* **132**, 733–744 (2007). doi:10.1053/j.gastro.2006.11.045 Medline

27. B. P. Doehle, A. Schäfer, B. R. Cullen, Human APOBEC3B is a potent inhibitor of HIV-1 infectivity and is resistant to HIV-1 Vif. *Virology* **339**, 281–288 (2005). doi:10.1016/j.virol.2005.06.005 Medline

28. G. Berger, J. Turpin, S. Cordeil, K. Tartour, X. N. Nguyen, R. Mahieux, A. Cimarelli, Functional analysis of the relationship between Vpx and the restriction factor SAMHD1. *J. Biol. Chem.* **287**, 41210–41217 (2012). doi:10.1074/jbc.M112.403816 Medline

29. H. Muckenfuss, M. Hamdorf, U. Held, M. Perkovic, J. Löwer, K. Cichutek, E. Flory, G. G. Schumann, C. Münk, APOBEC3 proteins inhibit human LINE-1 retrotransposition. *J. Biol. Chem.* **281**, 22161–22172 (2006). doi:10.1074/jbc.M601716200 Medline

30. C. Münk, A. Willemsen, I. G. Bravo, An ancient history of gene duplications, fusions and losses in the evolution of APOBEC3 mutators in mammals. *BMC Evol. Biol.* **12**, 71 (2012). doi:10.1186/1471-2148-12-71 Medline

31. M. A. Carpenter, M. Li, A. Rathore, L. Lackey, E. K. Law, A. M. Land, B. Leonard, S. M. Shandilya, M. F. Bohn, C. A. Schiffer, W. L. Brown, R. S. Harris, Methylcytosine and normal cytosine deamination by the foreign DNA restriction enzyme APOBEC3A. *J. Biol. Chem.* **287**, 34801–34808 (2012). doi:10.1074/jbc.M112.385161 Medline

32. P. Turelli, B. Mangeat, S. Jost, S. Vianin, D. Trono, Inhibition of hepatitis B virus replication by APOBEC3G. *Science* **303**, 1829 (2004). doi:10.1126/science.1092066 Medline

33. C. T. Bock, S. Schwinn, S. Locarnini, J. Fyfe, M. P. Manns, C. Trautwein, H. Zentgraf, Structural organization of the hepatitis B virus minichromosome. *J. Mol. Biol.* **307**, 183–196 (2001). doi:10.1006/jmbi.2000.4481 Medline

34. M. M. Aynaud, R. Suspène, P. O. Vidalain, B. Mussil, D. Guétard, F. Tangy, S. Wain-Hobson, J. P. Vartanian, Human Tribbles 3 protects nuclear DNA from cytidine deamination by APOBEC3A. *J. Biol. Chem.* **287**, 39182–39192 (2012). doi:10.1074/jbc.M112.372722 Medline

35. Y. Guo, W. Kang, X. Lei, Y. Li, A. Xiang, Y. Liu, J. Zhao, J. Zhang, Z. Yan, Hepatitis B viral core protein disrupts human host gene expression by binding to promoter regions. *BMC Genomics* **13**, 563 (2012). doi:10.1186/1471-2164-13-563 Medline

36. H. C. Smith, R. P. Bennett, A. Kizilyer, W. M. McDougall, K. M. Prohaska, Functions and regulation of the APOBEC family of proteins. *Semin. Cell Dev. Biol.* **23**, 258–268 (2012). doi:10.1016/j.semcdb.2011.10.004 Medline

37. T. H. Lee, S. J. Elledge, J. S. Butel, Hepatitis B virus X protein interacts with a probable cellular DNA repair protein. *J. Virol.* **69**, 1107–1114 (1995). Medline

38. K. Kitamura, Z. Wang, S. Chowdhury, M. Simadu, M. Koura, M. Muramatsu, Uracil DNA glycosylase counteracts APOBEC3G-induced hypermutation of hepatitis B viral genomes: excision repair of covalently closed circular DNA. *PLoS Pathog.* **9**, e1003361 (2013). doi:10.1371/journal.ppat.1003361 Medline

39. S. Landry, I. Narvaiza, D. C. Linfesty, M. D. Weitzman, APOBEC3A can activate the DNA damage response and cause cell-cycle arrest. *EMBO Rep.* **12**, 444–450 (2011). doi:10.1038/embor.2011.46 Medline

40. M. B. Burns, L. Lackey, M. A. Carpenter, A. Rathore, A. M. Land, B. Leonard, E. W. Refsland, D. Kotandeniya, N. Tretyakova, J. B. Nikas, D. Yee, N. A. Temiz, D. E. Donohue, R. M. McDougle, W. L. Brown, E. K. Law, R. S. Harris, APOBEC3B is an enzymatic source of mutation in breast cancer. *Nature* **494**, 366–370 (2013). doi:10.1038/nature11881 Medline

41. K. Krebs, N. Böttinger, L. R. Huang, M. Chmielewski, S. Arzberger, G. Gasteiger, C. Jäger, E. Schmitt, F. Bohne, M. Aichler, W. Uckert, H. Abken, M. Heikenwalder, P. Knolle, U. Protzer, T cells expressing a chimeric antigen receptor that binds hepatitis B virus envelope proteins control virus replication in mice. *Gastroenterology* **145**, 456–465 (2013). doi:10.1053/j.gastro.2013.04.047 Medline

42. J. Lucifora, S. Arzberger, D. Durantel, L. Belloni, M. Strubin, M. Levrero, F. Zoulim, O. Hantz, U. Protzer, Hepatitis B virus X protein is essential to initiate and maintain virus replication after infection. *J. Hepatol.* **55**, 996–1003 (2011). doi:10.1016/j.jhep.2011.02.015 Medline

43. H. Schulze-Bergkamen, A. Untergasser, A. Dax, H. Vogel, P. Büchler, E. Klar, T. Lehnert, H. Friess, M. W. Büchler, M. Kirschfink, W. Stremmel, P. H. Krammer, M. Müller, U. Protzer, Primary human hepatocytes—a valuable tool for investigation of apoptosis and hepatitis B virus infection. *J. Hepatol.* **38**, 736–744 (2003). doi:10.1016/S0168-8278(03)00120-X Medline

44. S. M. Lee, C. Schelcher, M. Demmel, M. Hauner, W. E. Thasler, Isolation of human hepatocytes by a two-step collagenase perfusion procedure. *J. Vis. Exp.* (79): (2013). Medline

45. W. E. Thasler, T. S. Weiss, K. Schillhorn, P. T. Stoll, B. Irrgang, K. W. Jauch, Charitable State-Controlled Foundation Human Tissue and Cell Research: Ethic and Legal Aspects in the Supply of Surgically Removed Human Tissue For Research in the Academic and Commercial Sector in Germany. *Cell Tissue Bank.* **4**, 49–56 (2003). doi:10.1023/A:1026392429112 Medline

46. O. Hantz, R. Parent, D. Durantel, P. Gripon, C. Guguen-Guillouzo, F. Zoulim, Persistence of the hepatitis B virus covalently closed circular DNA in HepaRG human hepatocyte-like cells. *J. Gen. Virol.* **90**, 127–135 (2009). doi:10.1099/vir.0.004861-0 Medline

47. M. Quasdorff, M. Hösel, M. Odenthal, U. Zedler, F. Bohne, P. Gripon, H. P. Dienes, U. Drebber, D. Stippel, T. Goeser, U. Protzer, A concerted action of HNF4alpha and HNF1alpha links hepatitis B virus replication to hepatocyte differentiation. *Cell. Microbiol.* **10**, 1478–1490 (2008). doi:10.1111/j.1462-5822.2008.01141.x Medline

48. U. Protzer, S. Seyfried, M. Quasdorff, G. Sass, M. Svorcova, D. Webb, F. Bohne, M. Hösel, P. Schirmacher, G. Tiegs, Antiviral activity and hepatoprotection by heme oxygenase-1 in hepatitis B virus infection. *Gastroenterology* **133**, 1156–1165 (2007). doi:10.1053/j.gastro.2007.07.021 Medline

49. A. Untergasser, U. Zedler, A. Langenkamp, M. Hösel, M. Quasdorff, K. Esser, H. P. Dienes, B. Tappertzhofen, W. Kolanus, U. Protzer, Dendritic cells take up viral antigens but do not support the early steps of hepatitis B virus infection. *Hepatology* **43**, 539–547 (2006). doi:10.1002/hep.21048 Medline

50. J. Summers, P. M. Smith, A. L. Horwich, Hepadnavirus envelope proteins regulate covalently closed circular DNA amplification. *J. Virol.* **64**, 2819–2824 (1990). Medline

51. W. Gao, J. Hu, Formation of hepatitis B virus covalently closed circular DNA: removal of genome-linked protein. *J. Virol.* **81**, 6164–6174 (2007). doi:10.1128/JVI.02721-06 Medline

52. G. K. Smyth, Linear models and empirical bayes methods for assessing differential expression in microarray experiments. *Stat. Appl. Genet. Mol. Biol.* **3**, Article3 (2004).

53. C. Banning, J. Votteler, D. Hoffmann, H. Koppensteiner, M. Warmer, R. Reimer, F. Kirchhoff, U. Schubert, J. Hauber, M. Schindler, A flow cytometry-based FRET assay to identify and analyse protein-protein interactions in living cells. *PLoS ONE* **5**, e9344 (2010). doi:10.1371/journal.pone.0009344 Medline

54. K. Arnold, L. Bordoli, J. Kopp, T. Schwede, The SWISS-MODEL workspace: a web-based environment for protein structure homology modelling. *Bioinformatics* **22**, 195–201 (2006). doi:10.1093/bioinformatics/bti770 Medline

55. S. A. Wynne, R. A. Crowther, A. G. Leslie, The crystal structure of the human hepatitis B virus capsid. *Mol. Cell* **3**, 771–780 (1999). doi:10.1016/S1097-2765(01)80009-5 Medline

56. I. J. Byeon *et al.*, NMR structure of human restriction factor APOBEC3A reveals substrate binding and enzyme specificity. *Nat. Commun.* **4**, 1890 (2013).

57. A. W. Ghoorah, M. D. Devignes, M. Smaïl-Tabbone, D. W. Ritchie, Protein docking using case-based reasoning. *Proteins* **81**, 2150–2158 (2013). doi:10.1002/prot.24433 Medline

58. R. A. Sayle, E. J. Milner-White, RASMOL: biomolecular graphics for all. *Trends Biochem. Sci.* **20**, 374–376 (1995). doi:10.1016/S0968-0004(00)89080-5 Medline

59. L. G. Guidotti, B. Matzke, H. Schaller, F. V. Chisari, High-level hepatitis B virus replication in transgenic mice. *J. Virol.* **69**, 6158–6169 (1995). Medline

60. M. Dandri, M. R. Burda, E. Török, J. M. Pollok, A. Iwanska, G. Sommer, X. Rogiers, C. E. Rogler, S. Gupta, H. Will, H. Greten, J. Petersen, Repopulation of mouse liver with human hepatocytes and in vivo infection with hepatitis B virus. *Hepatology* **33**, 981–988 (2001). doi:10.1053/jhep.2001.23314 Medline

61. M. Lütgehetmann, T. Bornscheuer, T. Volz, L. Allweiss, J. H. Bockmann, J. M. Pollok, A. W. Lohse, J. Petersen, M. Dandri, Hepatitis B virus limits response of human hepatocytes to interferon-α in chimeric mice. *Gastroenterology* **140**, 2074–2083, e1–e2 (2011). doi:10.1053/j.gastro.2011.02.057 Medline

62. M. Sarasin-Filipowicz, E. J. Oakeley, F. H. Duong, V. Christen, L. Terracciano, W. Filipowicz, M. H. Heim, Interferon signaling and treatment outcome in chronic hepatitis C. *Proc. Natl. Acad. Sci. U.S.A.* **105**, 7034–7039 (2008). doi:10.1073/pnas.0707882105 Medline

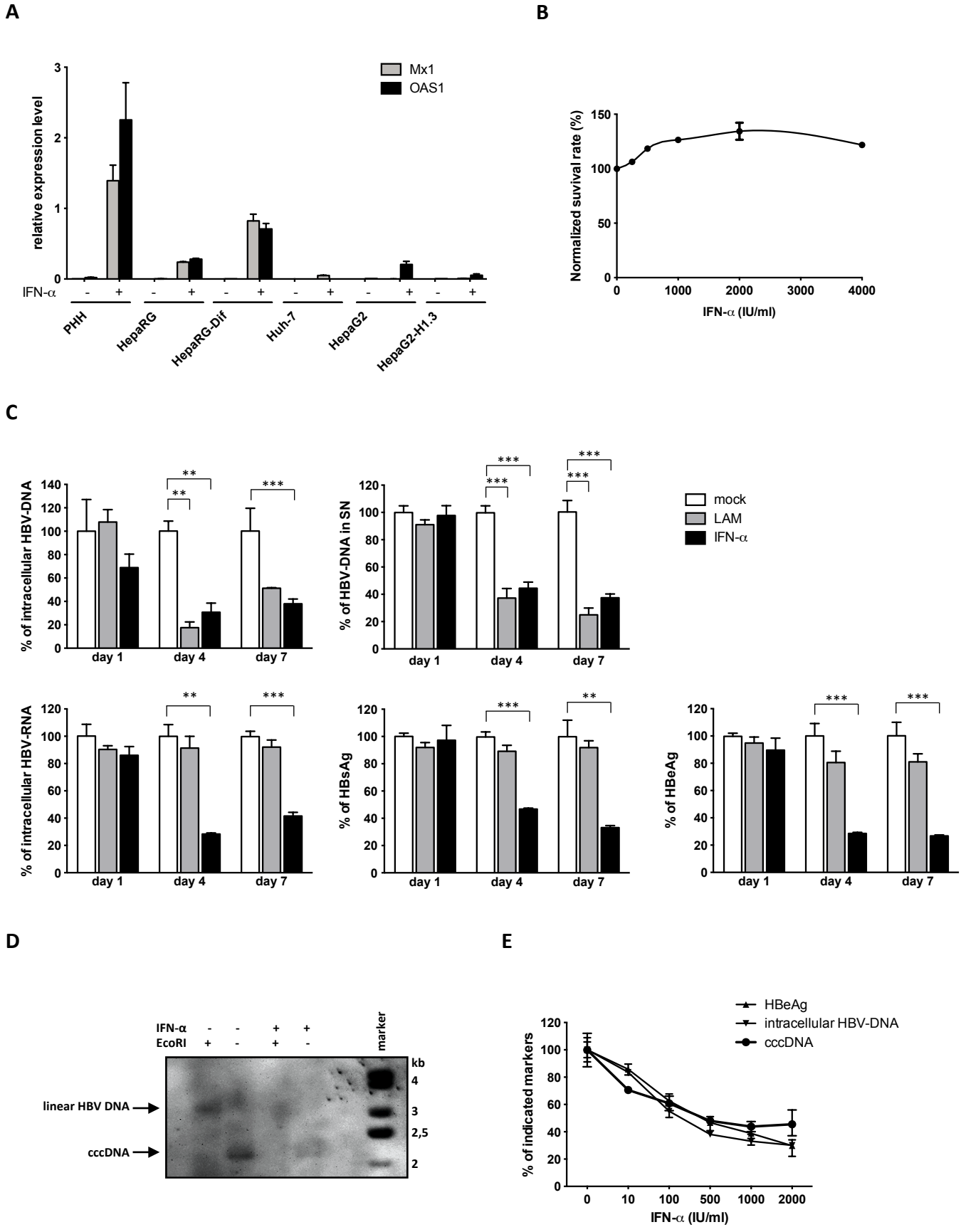

Figure S1. (A) The indicated cells were treated with IFN-α for 6 hours and levels of Mx1 and OAS1 were assessed by qRT-PCR. **(B, C)** dHepaRG cells were infected with HBV and treated 10 days later with IFN-α or Lamivudine (LAM). **(B)** Viability of cells was assessed by XTT test. **(C)** Levels of HBeAg, intracellular HBV-DNA, HBV-RNA or HBV-DNA in the supernatants were analyzed and compared to untreated cells (mock). Values given are the mean +/- standard deviation of biological triplicates and were analyzed by t-test. ** p<0.01 and *** p<0.001. **(D)** HBV cccDNA levels were analyzed by Southern blot 10 days post-treatment. Supercoiled cccDNA bands were identified by their expected size and ability to be linearized upon EcoRI digestion (3.2 kb). **(E)** Dose response curve of viral markers after IFN-α treatment for 7 days.

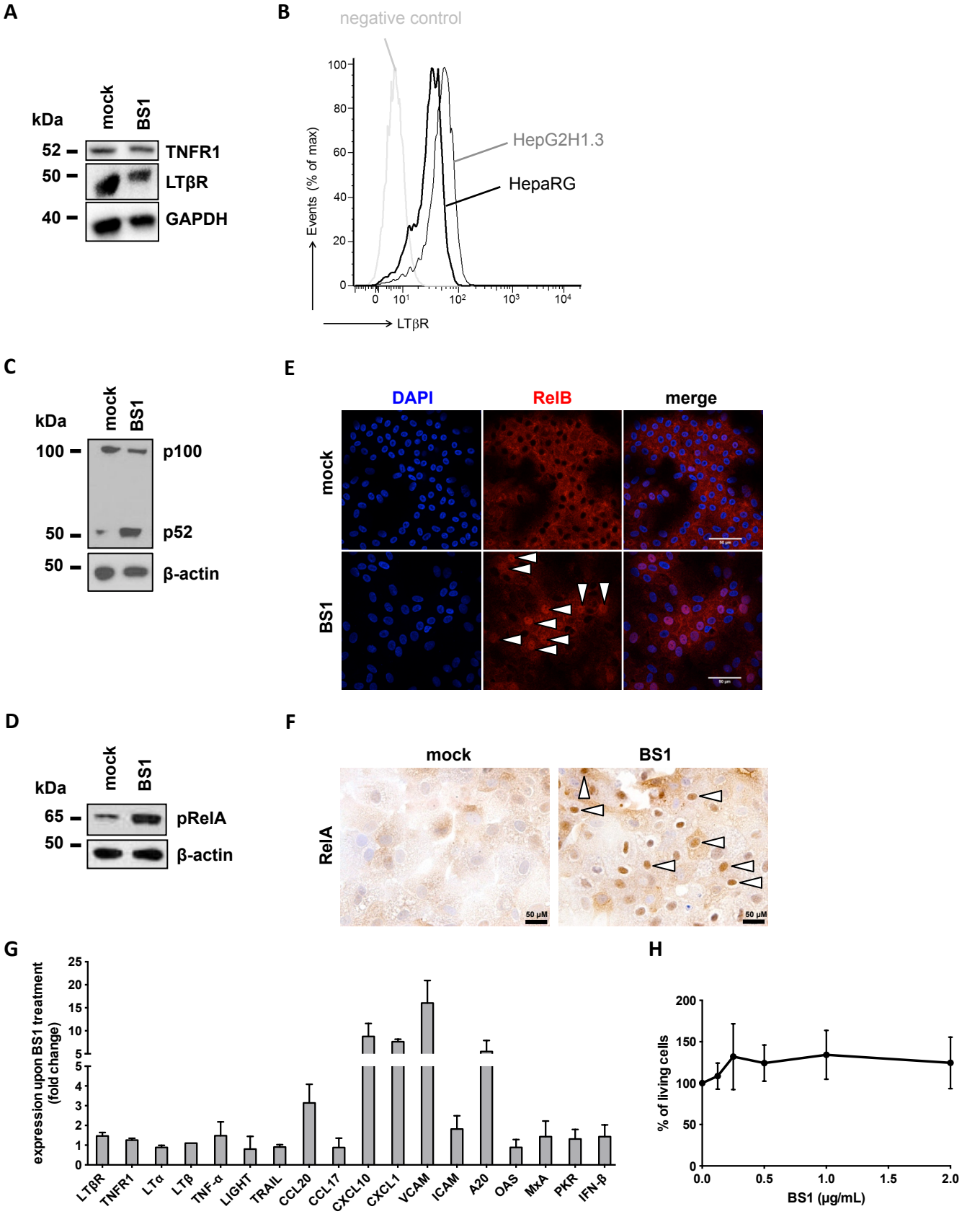

Figure S2. HBV-infected dHepaRG cells were treated with BS1. After 10 days, we analyzed **(A)** expression of LTβR and TNFR1 by Western blot and **(B)** by FACS analyses as well as **(C)** p100/p52 processing and **(D)** phosphorylation of RelA (pRelA) by Western blot. **(D)** Nuclear translocation of RelB and of **(F)** RelA by immunohistochemistry (white arrow heads indicate nuclear translocation in hepatocytes). **(G)** Expression analysis of indicated genes upon BS1 treatment by qRT-PCR. **(H)** Assessment of cell viability under different concentration of BS1 by XTT tests.

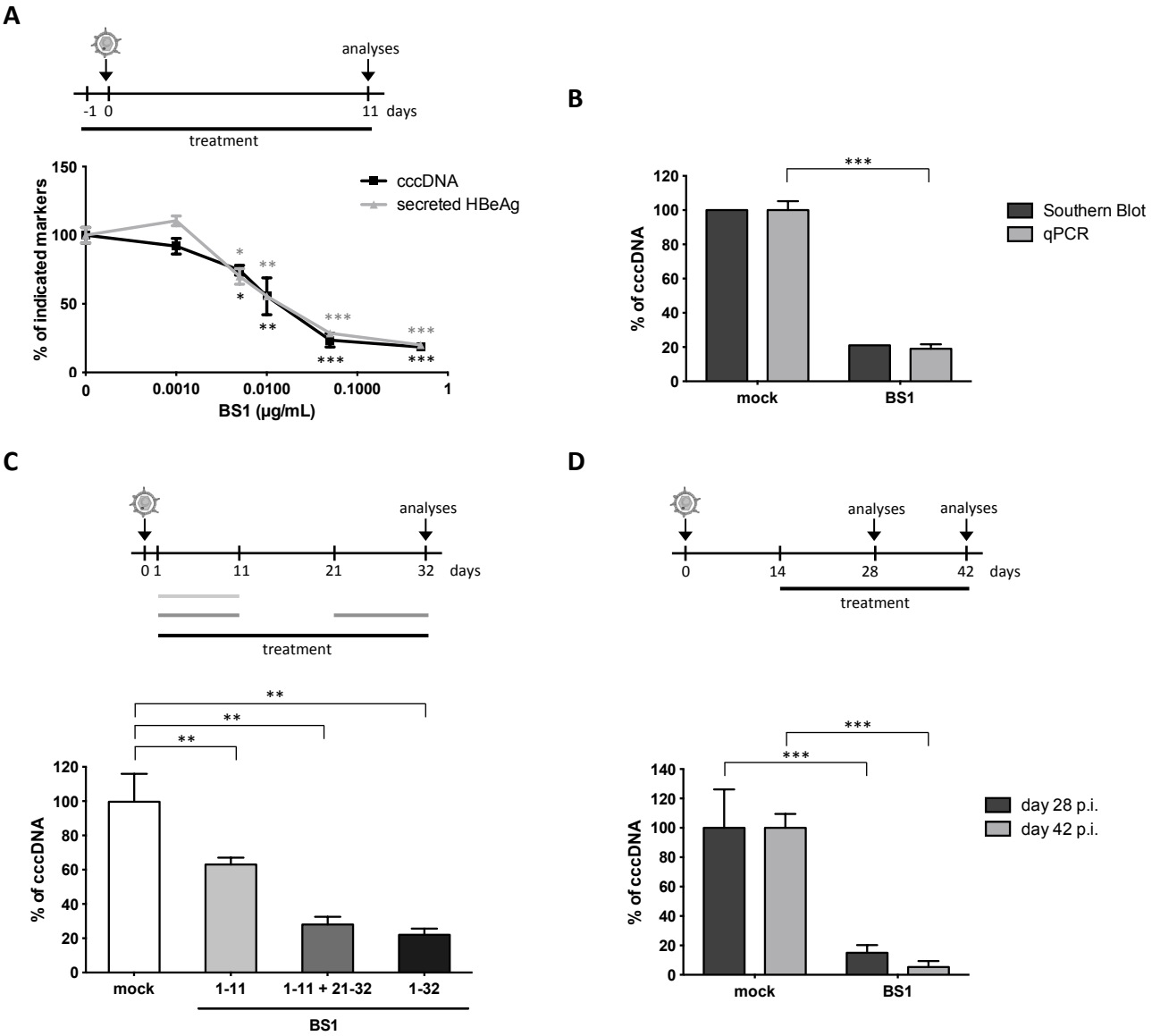

Figure S3. dHepaRG cells were infected with HBV and treated with LTβR-agonist BS1. **(A)** Dose response curve of viral markers upon BS1 treatment. **(B)** cccDNA signal detected by Southern blot analysis was quantified using a phosphorimager and compared to quantification of cccDNA of the same extract by qPCR. (**C, D**) HBV-infected dHepaRG cells were treated with BS1 as indicated in the schemes. cccDNA was quantified by qPCR relative to untreated cells (mock). Values are the mean +/- standard deviation of different replicates and data were analyzed by t-test. ** $p<0.01$ and *** $p<0.001$.

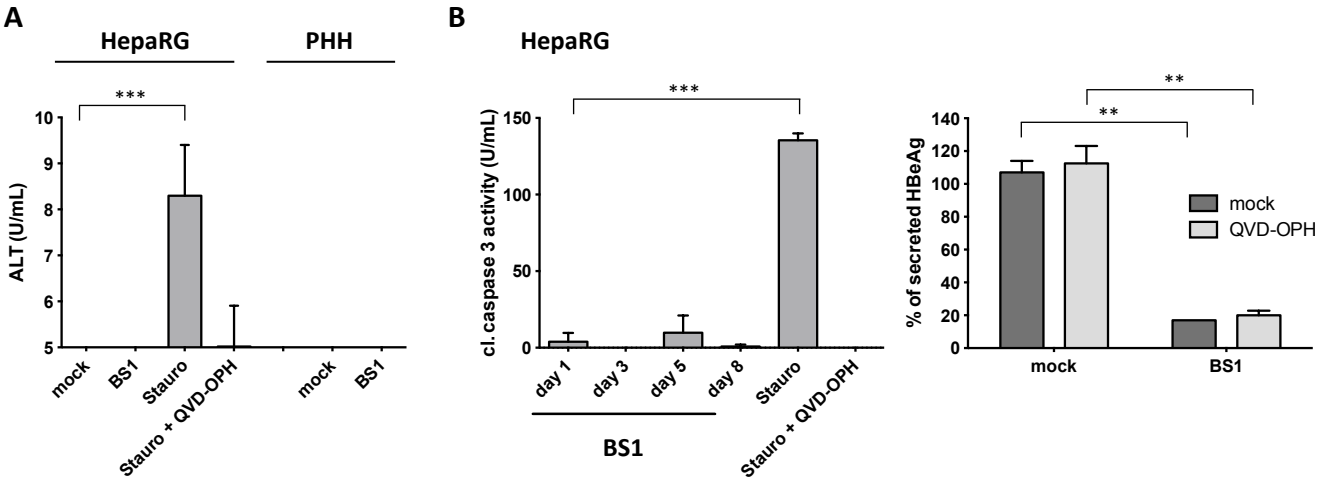

Figure S4. dHepaRG cells or primary human hepatocytes (PHH) were infected with HBV and treated with BS1 for 11 days and assayed for apoptosis induction. As positive control, cells were treated 12h before the end of the experiment with 1 µg/mL of Staurosporine (Stauro). ALT **(A)** and HBeAg levels **(B, right panel)** were quantified in the supernatant. Cleaved caspase 3 activity was analyzed **(B, left panel)**.

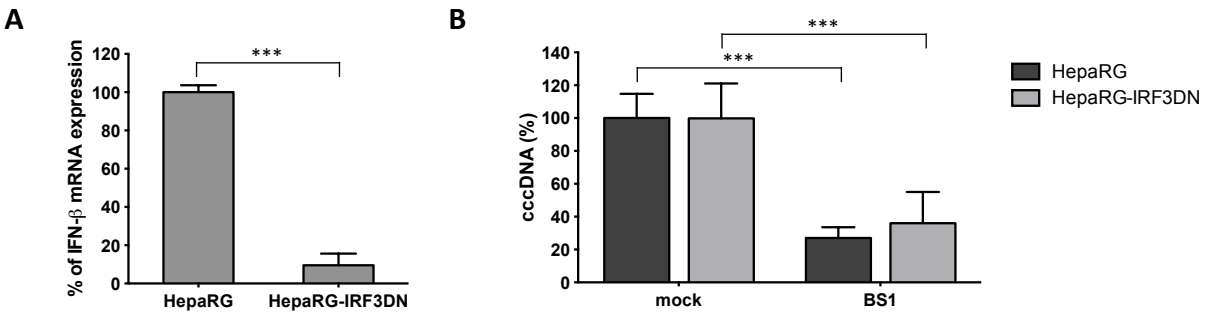

Figure S5. To exclude induction of IFN responses, HepaRG cells expressing a dominant negative version of the IFN regulated factor 3 (IRF3) were generated. (**A)** dHepaRG and dHepaRGIRF3DN cells were stimulated with poly-IC during 8h and expression of IFN-β was analyzed by qRT-PCR (relative to GAPDH). **(B)** dHepaRG or dHepaRGIRF3DN cells were infected with HBV and treated with BS1 24h later and for 10 days. cccDNA content was analyzed and expressed in % of untreated cells (mock). Values are given as mean +/- standard deviation of three replicates and data were analyzed by t-test. ** $p<0.01$ and *** $p<0.001$.

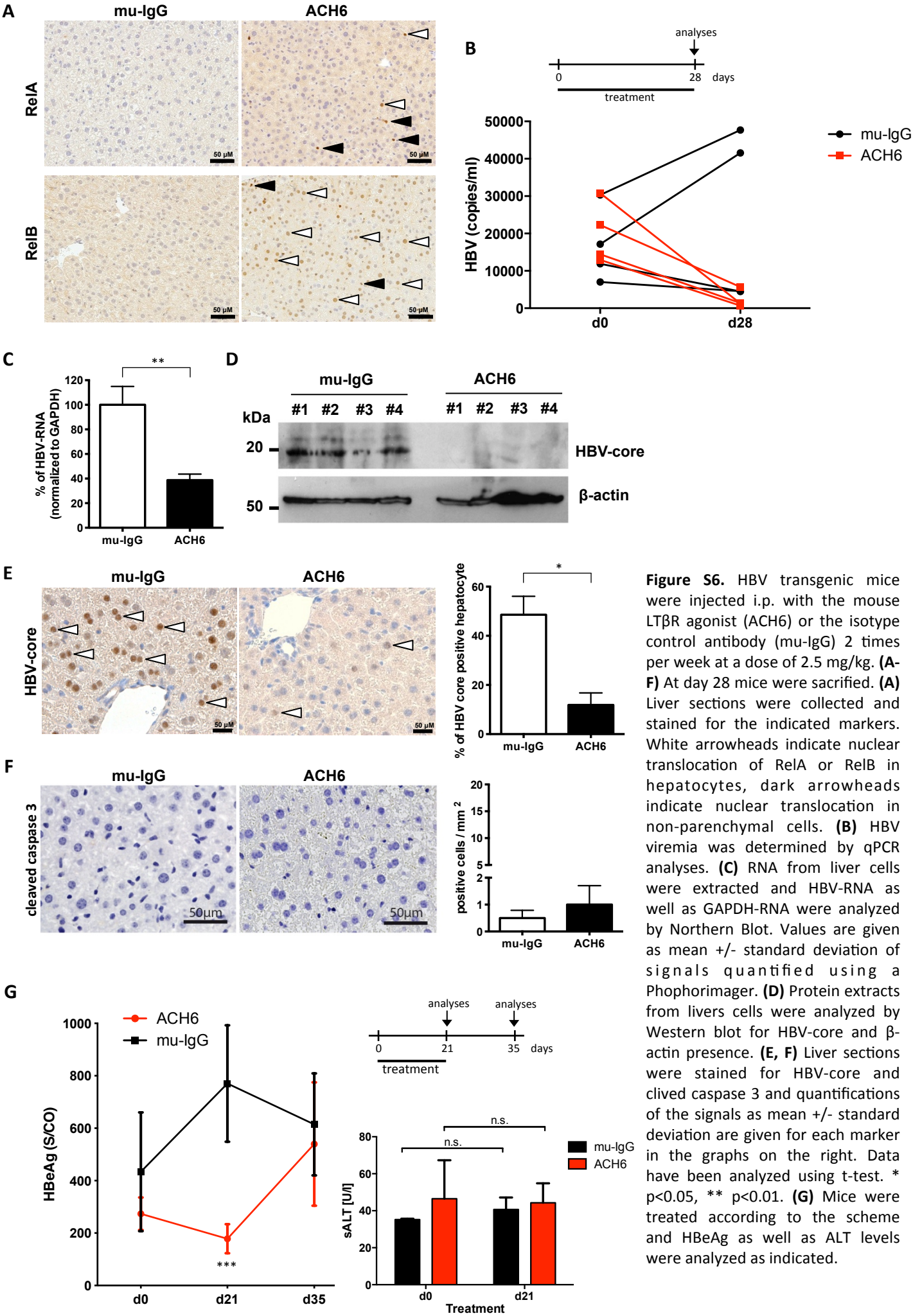

Figure S6. HBV transgenic mice were injected i.p. with the mouse LTβR agonist (ACH6) or the isotype control antibody (mu-IgG) 2 times per week at a dose of 2.5 mg/kg. **(A-F)** At day 28 mice were sacrified. **(A)** Liver sections were collected and stained for the indicated markers. White arrowheads indicate nuclear translocation of RelA or RelB in hepatocytes, dark arrowheads indicate nuclear translocation in non-parenchymal cells. **(B)** HBV viremia was determined by qPCR analyses. **(C)** RNA from liver cells were extracted and HBV-RNA as well as GAPDH-RNA were analyzed by Northern Blot. Values are given as mean +/- standard deviation of signals quantified using a Phophorimager. **(D)** Protein extracts from livers cells were analyzed by Western blot for HBV-core and β-actin presence. **(E, F)** Liver sections were stained for HBV-core and clived caspase 3 and quantifications of the signals as mean +/- standard deviation are given for each marker in the graphs on the right. Data have been analyzed using t-test. * $p<0.05$, ** $p<0.01$. **(G)** Mice were treated according to the scheme and HBeAg as well as ALT levels were analyzed as indicated.

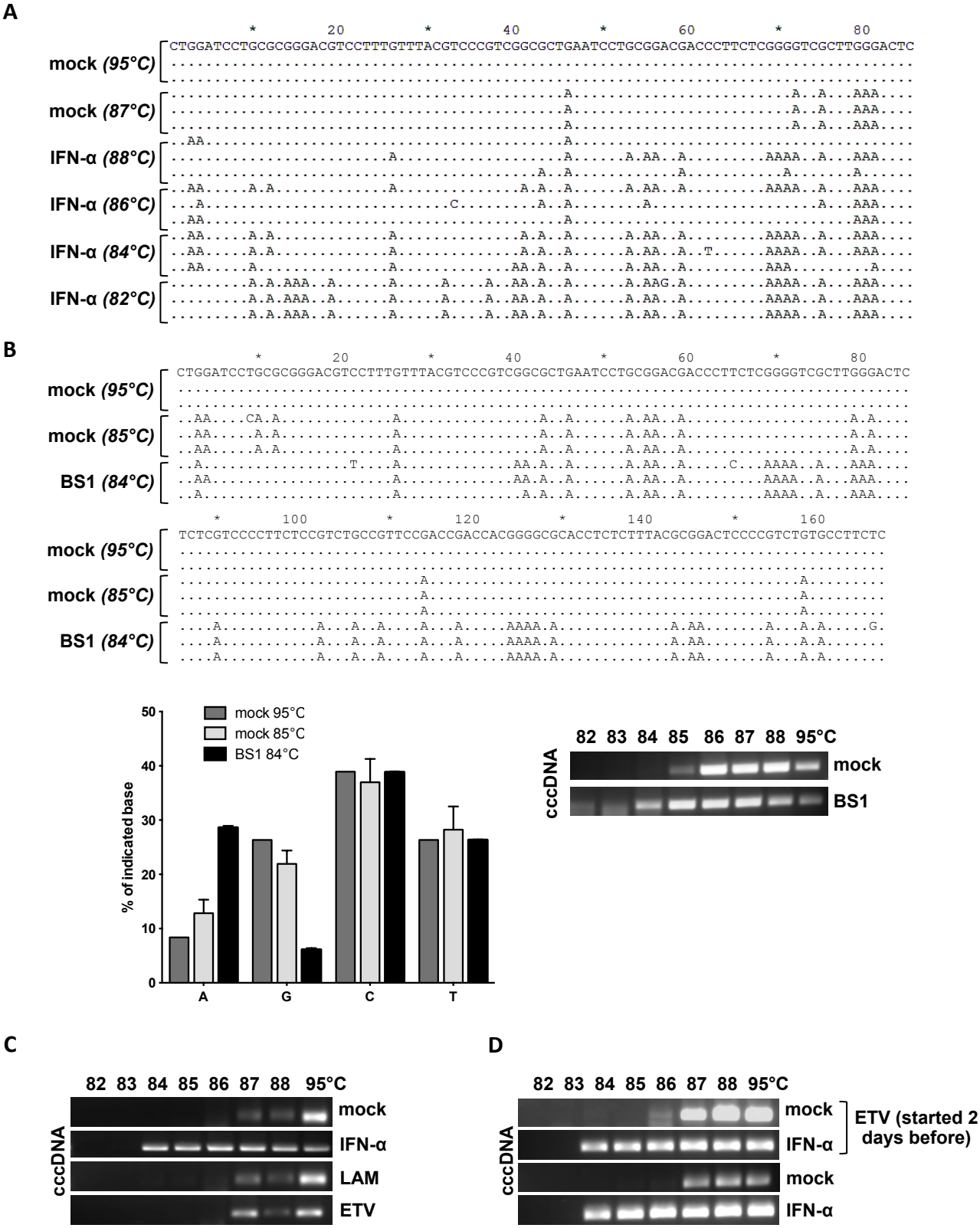

Figure S7. HBV-infected dHepaRG cells were treated with **(A)** IFN-α or **(B)** LTβR-agonist BS1, for 10 days. 3D-PCRs analyses were performed on cccDNA. **(A, B)** 3D-PCR products obtained at indicated temperatures were cloned, sequenced and numbers of G/A mutations were evaluated. (**C)** 3D-PCR of cccDNA after 10 days of treatment with IFN-α or nucleoside analogues lamivudine (LAM) or entecavir (ETV). **(D)** Treatment with IFN-α alone was compared to combined IFN-α+ETV treatment.

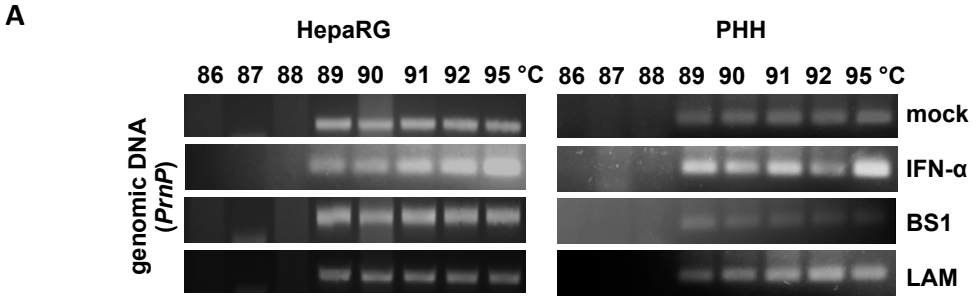

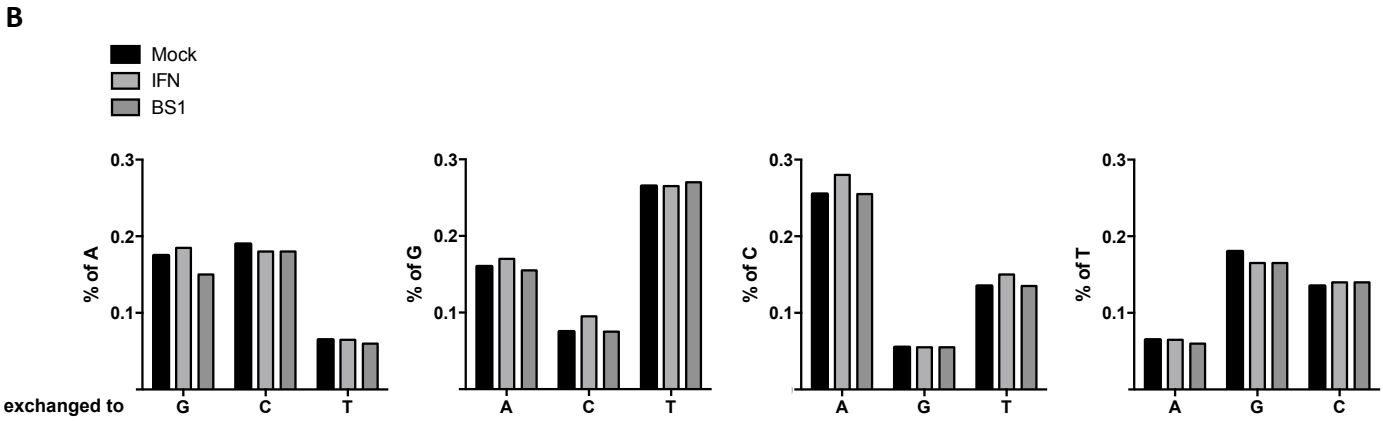

C

Gene Name	Amplicon Length	Genomic Position	% GC	Average coverage	% overall Mutation Rate (Mock/IFN/BS1)	G-A Mutation Rate (Mock/IFN/BS1)	C-T Mutation Rate (Mock/IFN/BS1)
B2M	2157	Chr. 15: 15798407 - 15800563	40,10	85 543	0.31/0.31/0.31	0.050/0.045/0.045	0.055/0.050/0.050
TBP	2249	Chr. 6: 75031948 - 75034196	47,13	134 116	0.32/0.32/0.31	0.055/0.055/0.050	0.055/0.055/0.055
HMBS	2372	Chr. 11: 22521107 - 22523478	52,40	124 475	0.45/0.44/0.45	0.18/0.18/0.18	0.23/0.23/0.23
MYC	1794	Chr. 8: 42024572 - 42026365	49,39	3 191	5.5/5.3/5.3	6.6/6.4/6.2	3.5/3.2/3.0
SRC	1863	Chr. 20: 6168000 - 6169862	52,76	120 392	0.41/0.40/0.40	0.14/0.14/0.14	0.055/0.050/0.050
MxA	1882	Chr. 21: 28473387 - 28475268	49,15	4 631	3.4/3.2/2.5	1.1/1.1/0.8	2.6/2.4/1.9
PKR	1713	Chr. 2: 16170524 - 16172236	42,97	115 858	0.69/0.65/0.66	0.25/0.22/0.24	0.32/0.29/0.31
PML	2084	Chr. 15: 45116397 - 45118480	53,50	50 881	0.48/0.58/0.39	0.16/0.20/0.13	0.080/0.10/0.055
CXCL10	1577	Chr. 4: 1490756 - 1492332	37,67	103 739	0.44/0.44/0.45	0.16/0.16/0.17	0.055/0.055/0.050
CXCL13	1884	Chr. 4: 3074754 - 3076637	37,58	114 082	0.31/0.30/0.30	0.055/0.055/0.055	0.055/0.055/0.055
CCL17	2124	Chr. 16: 11062012 - 11064135	56,36	87 806	0.71/0.74/0.74	0.27/0.30/0.29	0.20/0.25/0.23
CCL20	1767	Chr. 2: 78889580 - 78891346	34,24	121 839	0.32/0.31/0.31	0.055/0.050/0.050	0.060/0.055/0.055
IL6	2070	Chr. 7: 22759130 - 22761199	45,17	118 519	0.41/0.45/0.41	0.13/0.13/0.12	0.11/0.15/0.11

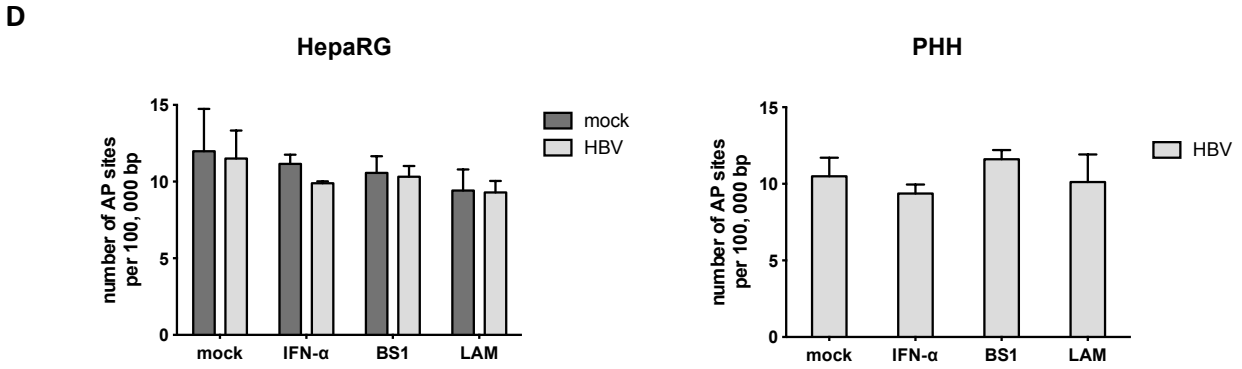

Figure S8. (A) dHepaRG cells or PHH were infected with HBV, treated with IFN-α or LTβR-agonist BS1 for 10 days and 3D-PCR analysis was performed on a region of the *PrnP* gene. **(B)** 13 different amplicons from different genomic DNA regions from cells treated with IFN-α or BS1 were submitted for deep sequencing. The overall % of base exchanged for each base was analyzed. (**C**) The table gives the genes analyzed, length and genomic position of the amplicons, the coverage rate as well as mutations rates. **(D)** dHepaRG cells or primary human hepatocyte (PHH) were infected with HBV or mock-infected and treated with IFN-α or BS1 4 days later for 10 days. Total DNA was extracted and AP sites were quantified. Values given are the mean +/- standard deviation of biological triplicates from one experiment.

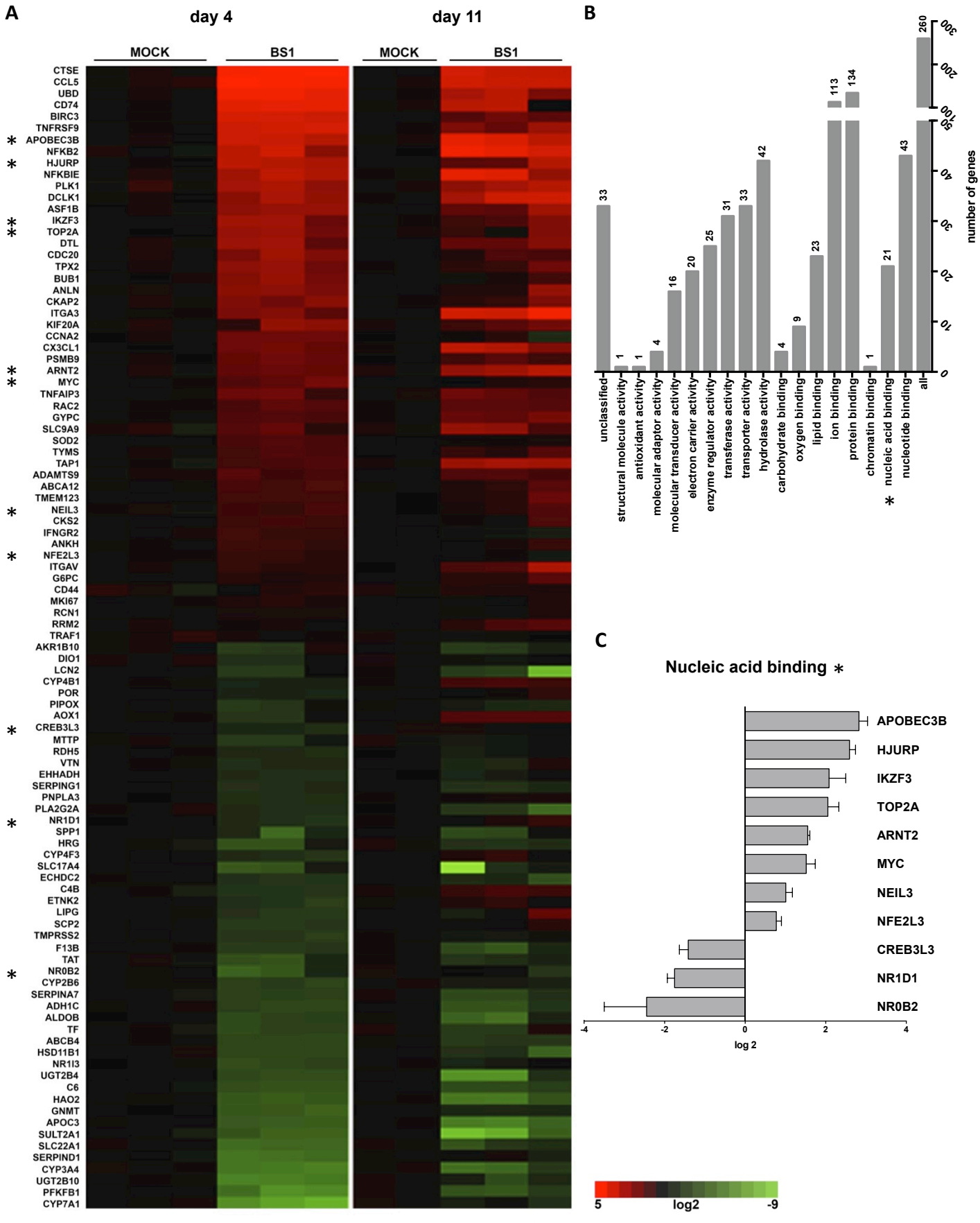

Figure S9. dHepaRG cells were infected with HBV and treated with LTβR-agonist BS1. **(A)** Affymetrix gene expression array analysis was confirmed by qRT-PCR analysis of the 50 most strongly up- and down-regulated genes. Results are shown as level of regulation according to the scale bars. **(B, C)** Regulated genes were classified according to their activity and binding properties. Stars indicate proteins for which nucleic acid binding properties have been described.

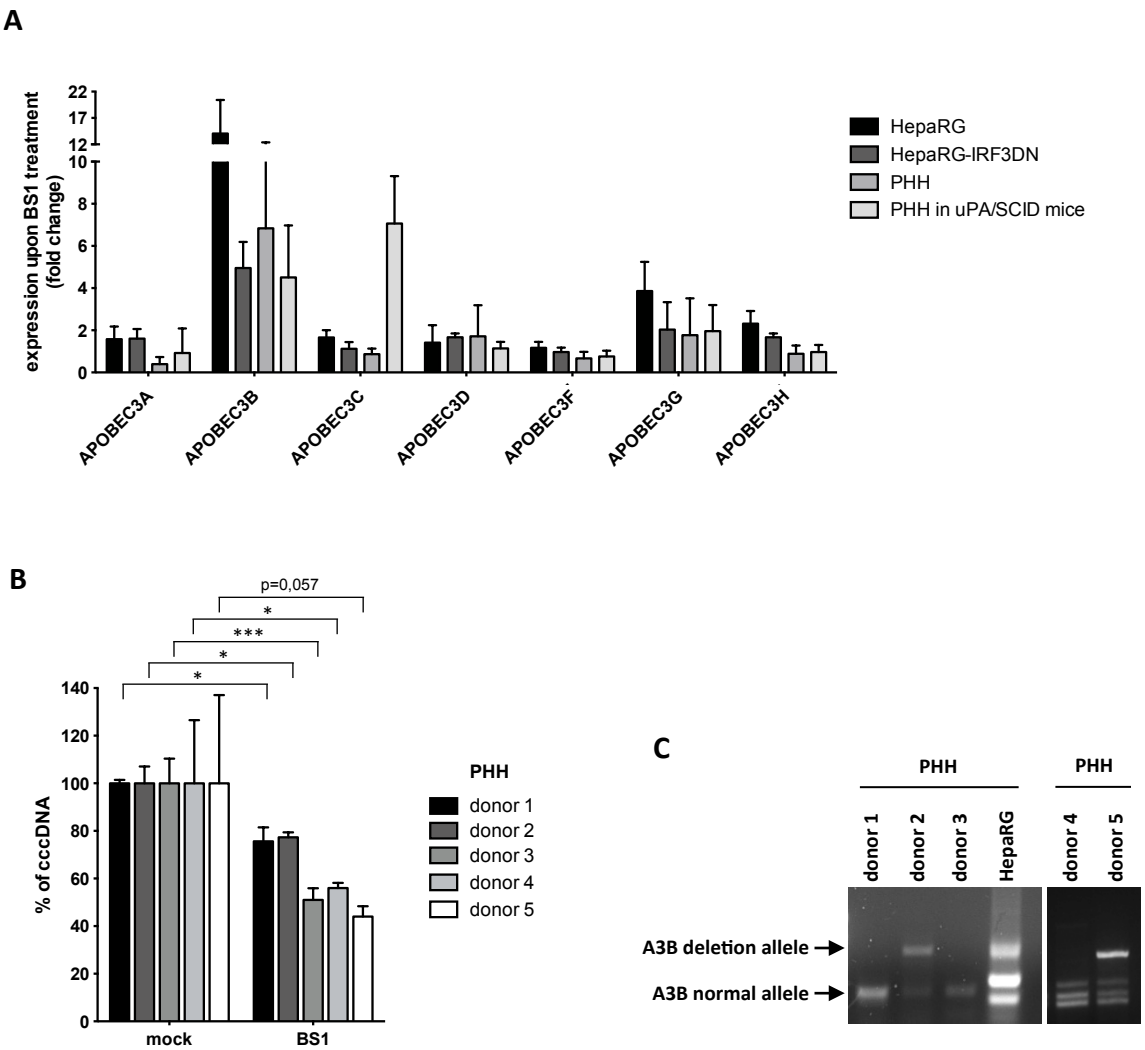

Figure S10. (A) Indicated cells were infected with HBV and treated with LTβR-agonist BS1 (dHepaRG, dHepaRG-IRF3DN: 10 days; PHH: 7 days; PHH in uPA/SCID mice: 2 weeks). Expression of APOBEC3 family members were analyzed by qRT-PCR and values are shown as mean +/- standard deviation of independent replicates. **(B)** PHH were infected with HBV and treated with BS1 at 7 dpi for 10 days. Levels of cccDNA were compared to untreated PHH of the same donor (mock). **(C)** PCR analysis to detect the wild-type A3B allele or a common deletion of the A3B allele in genomic DNA extracted from PHH derived from different donors as well as from HepaRG cells.

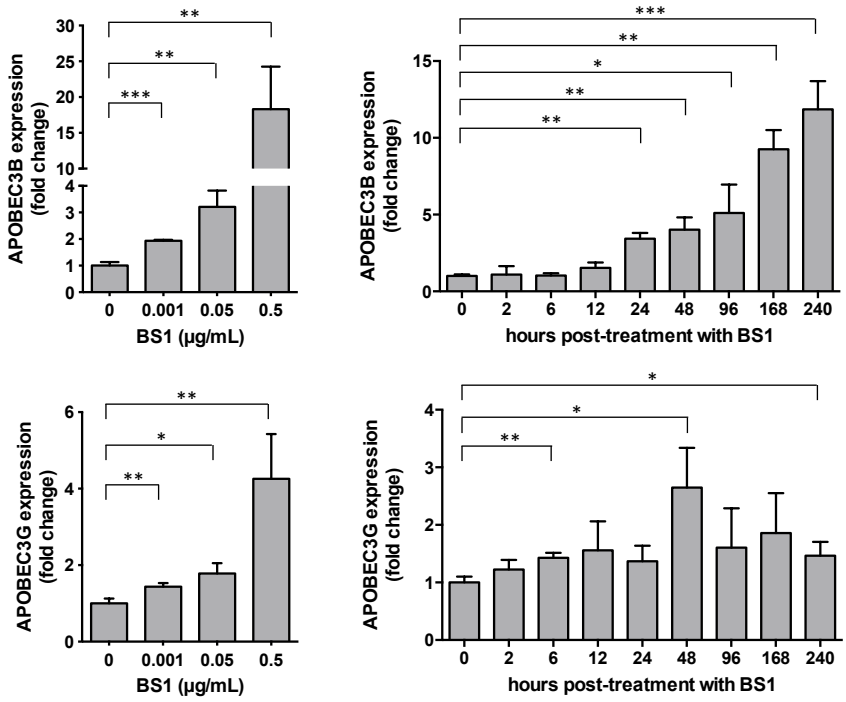

Figure S11. dHepaRG cells were infected with HBV and treated with LTβR-agonist BS1. Expression levels of APOBEC3B and APOBEC3G after 10 days or at indicated time points were analyzed by qRT-PCR. Values show mean +/- standard deviation of independent replicates and data and were analyzed by t-test. * $p<0.05$, ** $p<0.01$ and *** $p<0.001$.

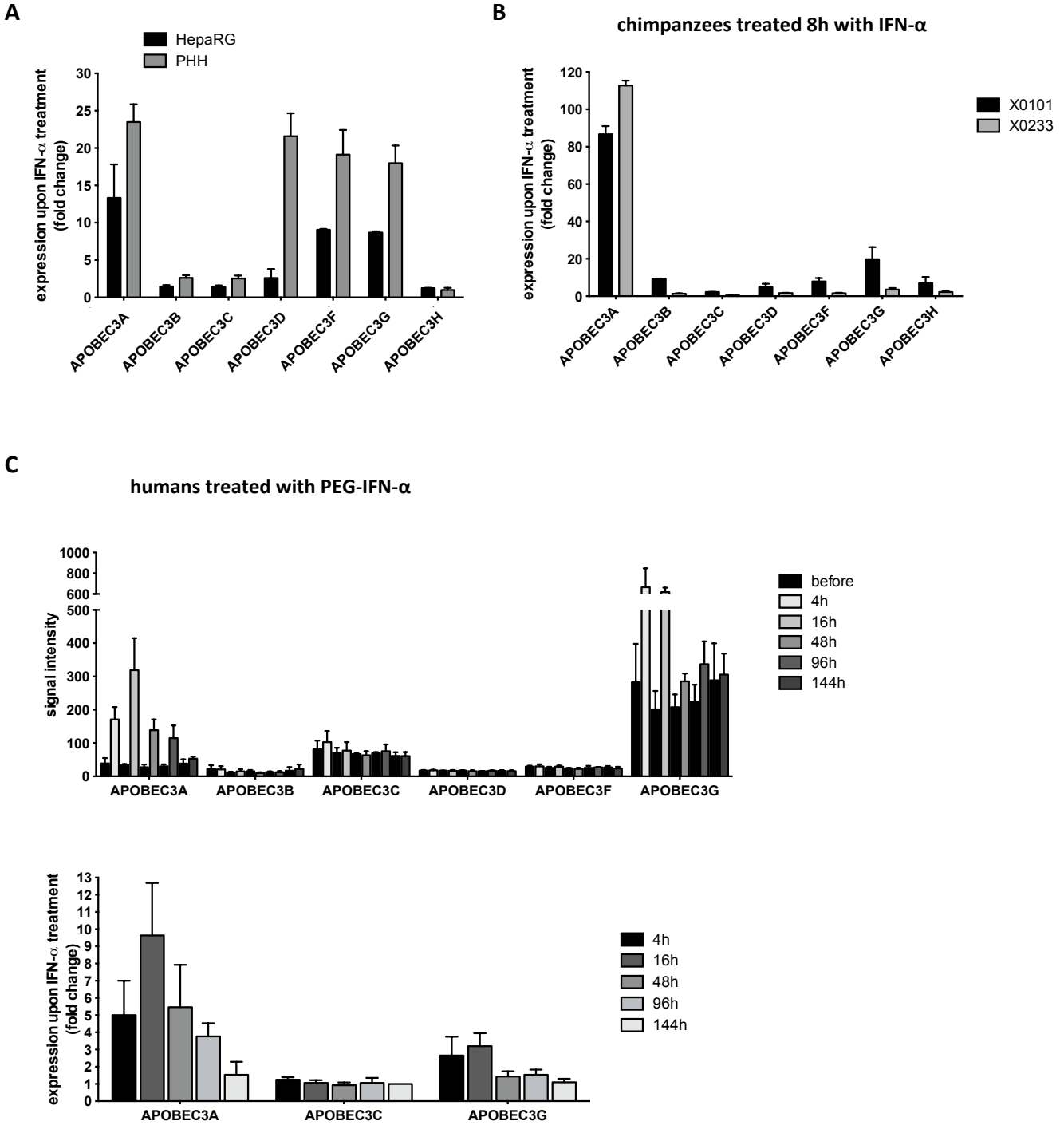

Figure S12. (A) Indicated cells were infected with HBV and treated with IFN-α for 6 hours. Expression of APOBEC3 family members was analyzed by qRT-PCR and values are shown as mean +/- standard deviation of independent replicates. **(B)** Chimpanzees X0101 and X0233 were treated with 10 million IU of recombinant human IFNα-2a. Liver biopsies were obtained 8 hrs post treatment and expression of APOBEC3 genes were analyzed. **(C)** RNA isolated from livers of HCV-patients (n=3 to 6 at different time points) before and after treatment with 1.5 µg/kg pegIFNα-2b were analyzed for the expression of APOBEC3 family members by gene expression array at indicated time points. Intensity values are given for the different APOBEC3 family members (upper graph) and fold changes were calculated when intensity values were above the threshold (lower graph).

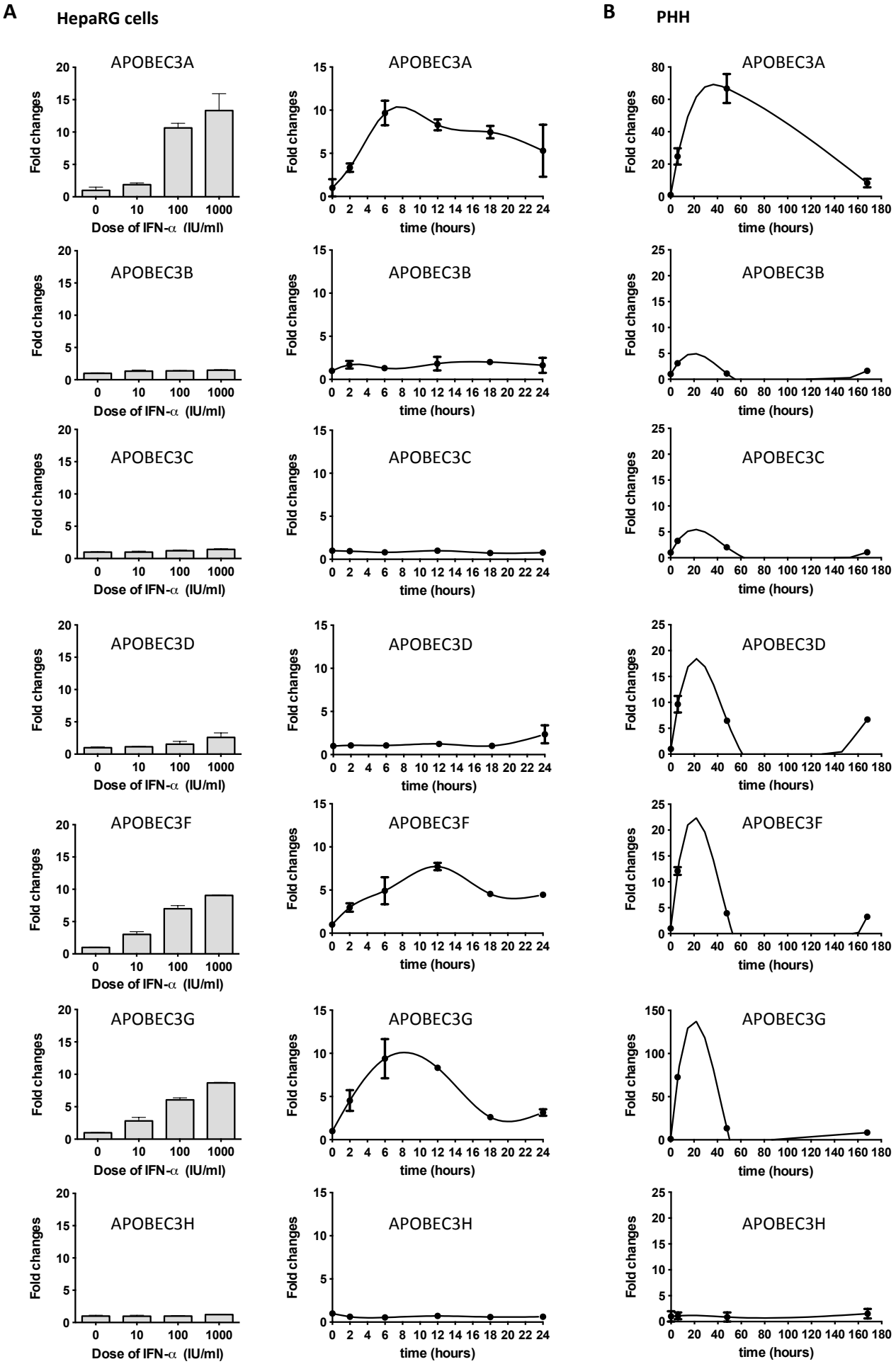

Figure S13. (A) dHepaRG cells or **(B)** PHH were infected with HBV and treated with IFN-α. Expression of the indicated APOBEC3 mRNA after 6h or at the indicated time point were analyzed by qRT-PCR. Values show mean +/- standard deviation of independent replicates.

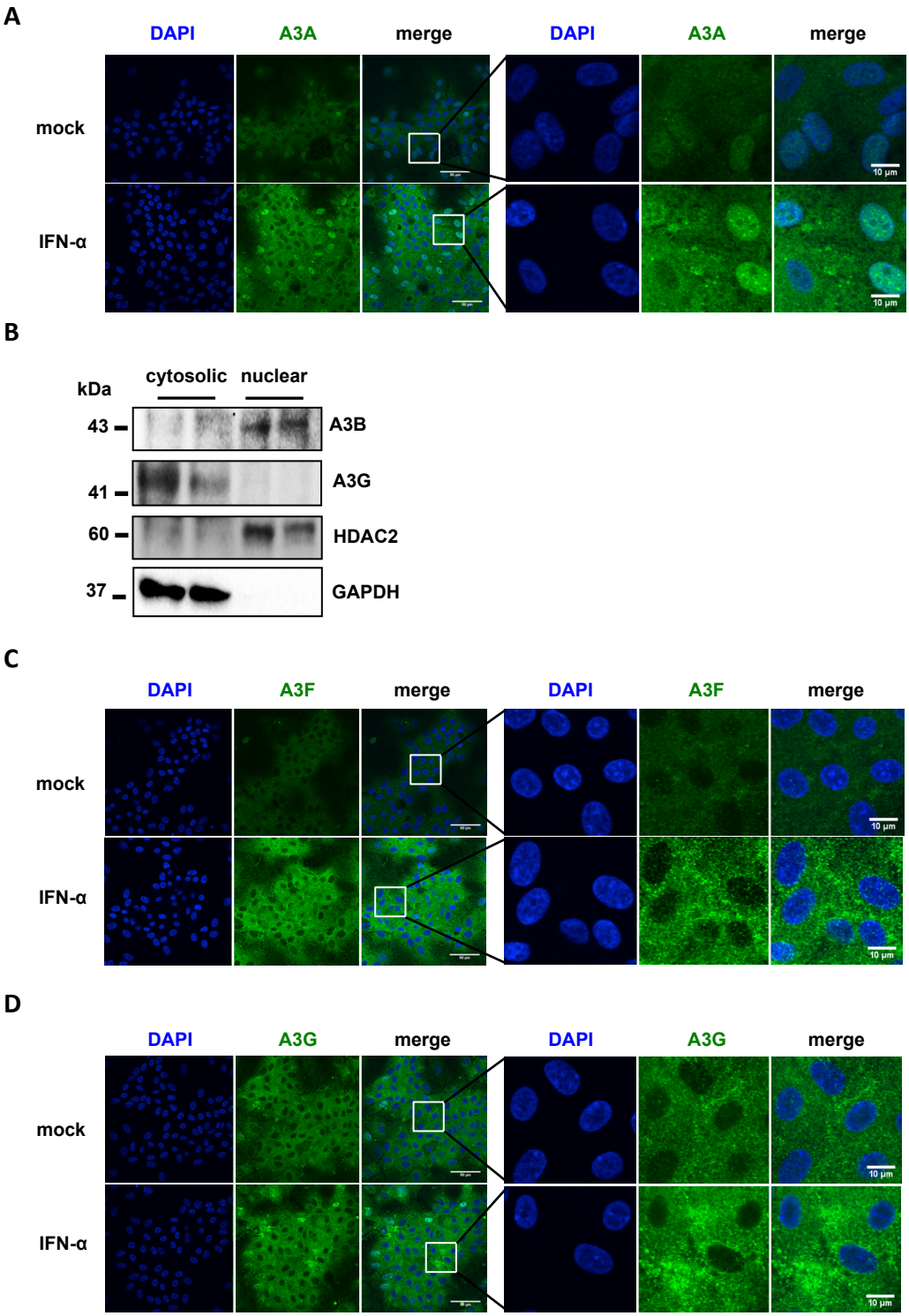

Figure S14. dHepaRG cells were treated with IFN-α or mock-treated and fixed three days later. A3A, A3B, A3F or A3G localization were determined by **(A, C, D)** immunofluorescence staining or **(B)** Western blot analysis.

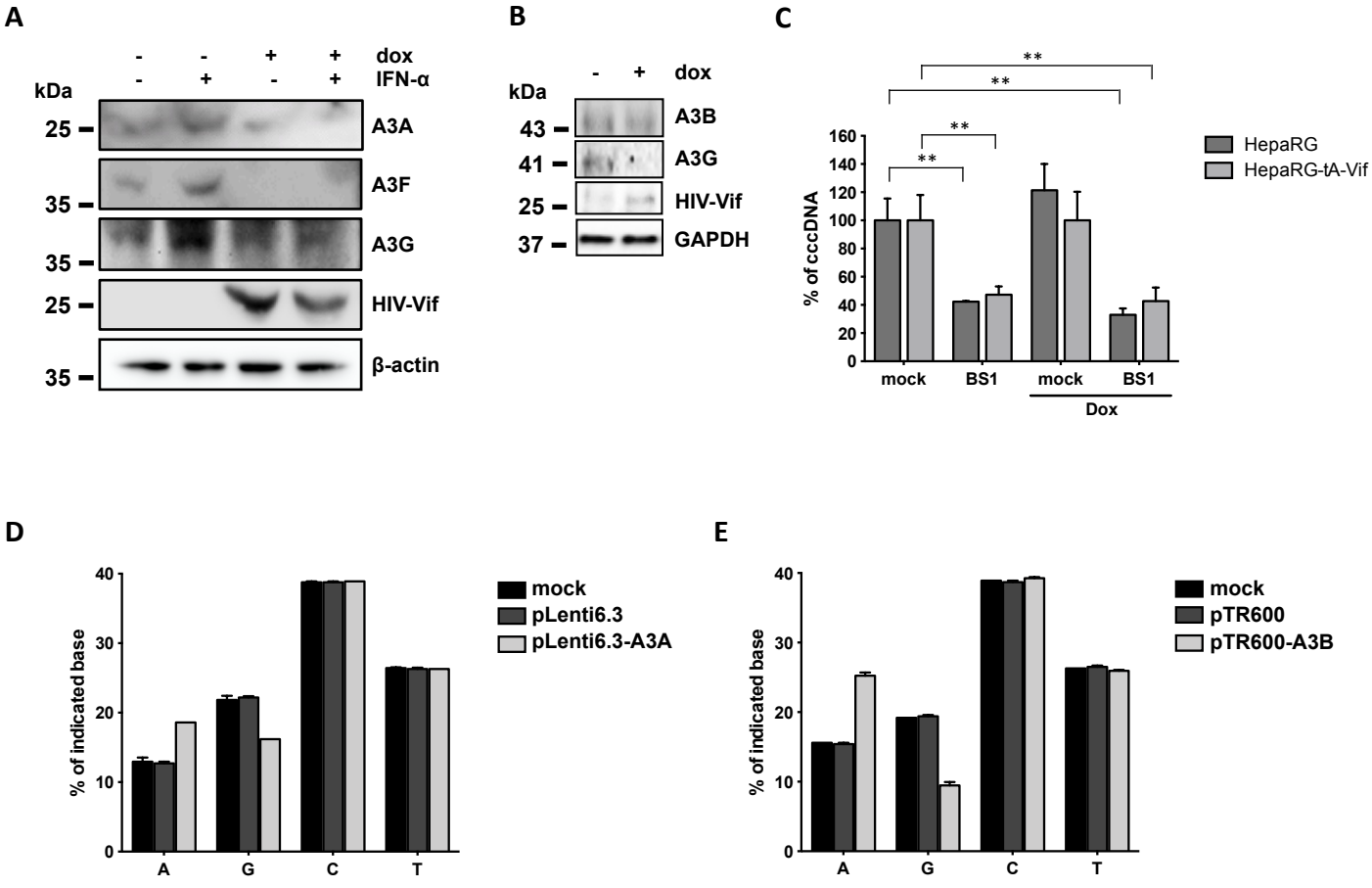

Figure S15. HBV-infected dHepaRG-tA-Vif cells were treated with **(A)** IFN-α or **(B, C)** LTβR-agonist BS1 for 10 days. 24h prior to HBV infection, HIV-Vif expression has been induced by doxycycline (dox). **(A, B)** Western blot analysis and **(C)** cccDNA qPCR were performed at the end of treatment. Values show the mean +/- standard deviation of independent replicates and data were analyzed by t-test.** $p<0.01$. **(D)** A3A and **(E)** A3B were overexpressed in HepG2-H1.3 cells. 3D-PCR experiments were performed 5 days later and the resulting PCR products were cloned and sequenced. Content of each base is given.

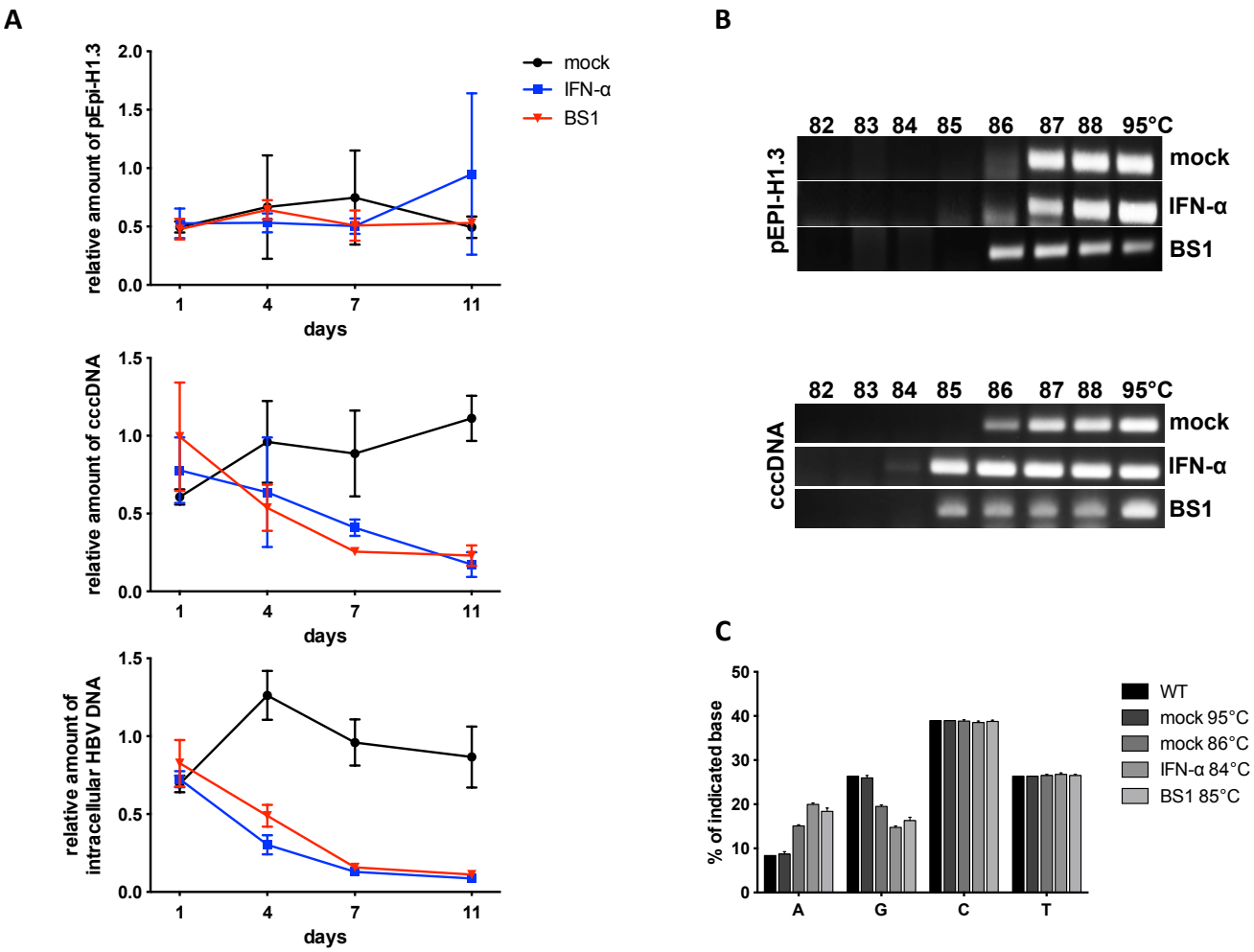

Figure S16. dHepaRG-pEpi-H1.3 cells were treated with IFN-α (500 IU/ml) or BS1 (0.5 µg/ml) for 11 days. (A) pEpi-H1.3 DNA, cccDNA and total intracellular HBV DNA were quantified by specific qPCR. (B) 3D-PCR specific for pEPIH.13 or cccDNA are shown. (C) HBV cccDNA 3D-PCR products obtained at indicated temperatures were cloned, sequenced and numbers of G/A mutations were evaluated.

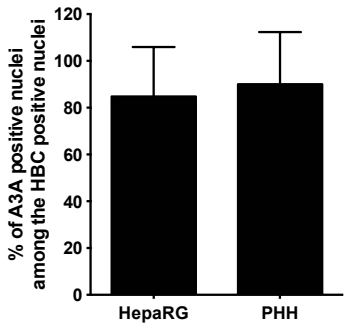

Figure S17. HBV-infected dHepaRG and PHH were treated with IFN-α at 7 dpi for 3 days. A3A and HBc were analyzed by immunofluorescence staining and quantification (mean ± SD) of A3A/HBc colocalisation in the nuclei from 5 different vision fields are given.

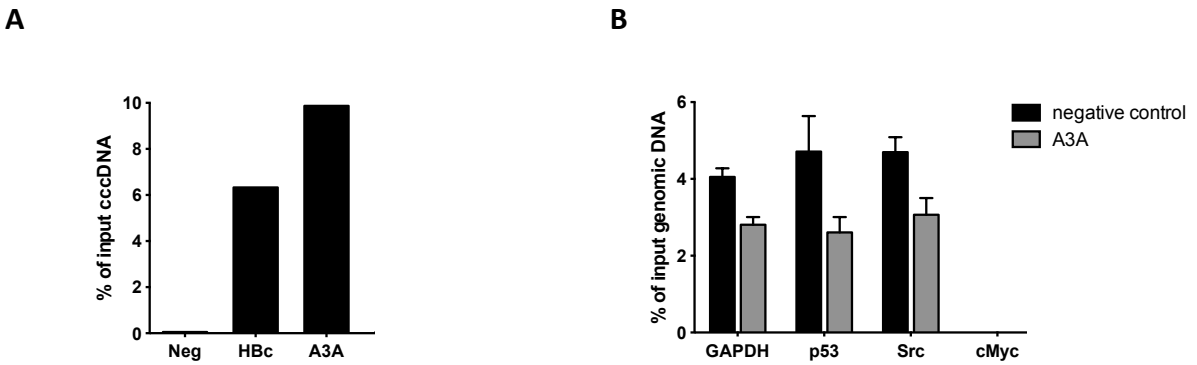

Figure S18. HepG2H1.3-A3A cells were analyzed by chromatin immunoprecipitation with anti-A3A, anti-HBc or using protein A/G beads only (negative control) and by qPCR using selective primers for (A) cccDNA (B) GAPDH, tumor suppressor p53, cellular/sarcoma tyrosine kinase (Src) and myelocytomatosis (c-myc).

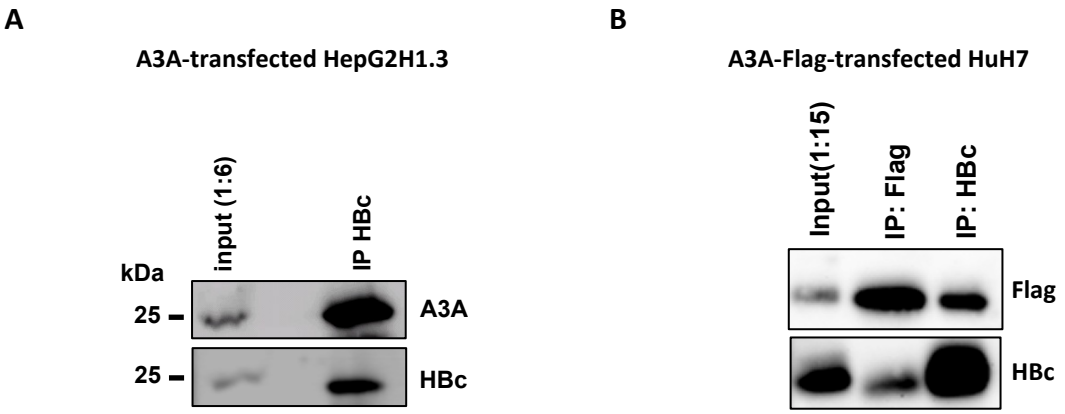

Figure S19. (A) HepG2H1.3 cells were transfected with a plasmid expressing A3A. (**B**) Huh-7 cells were co-transfected with a plasmid expressing A3A-Flag and one containing a 1.1-fold HBV genome expressing all HBV genes. After 72h, cells were lysed and the indicated immunoprecipitations (IP) followed by Western blot for the A3A, Flag tag and HBV core (HBc) were performed.

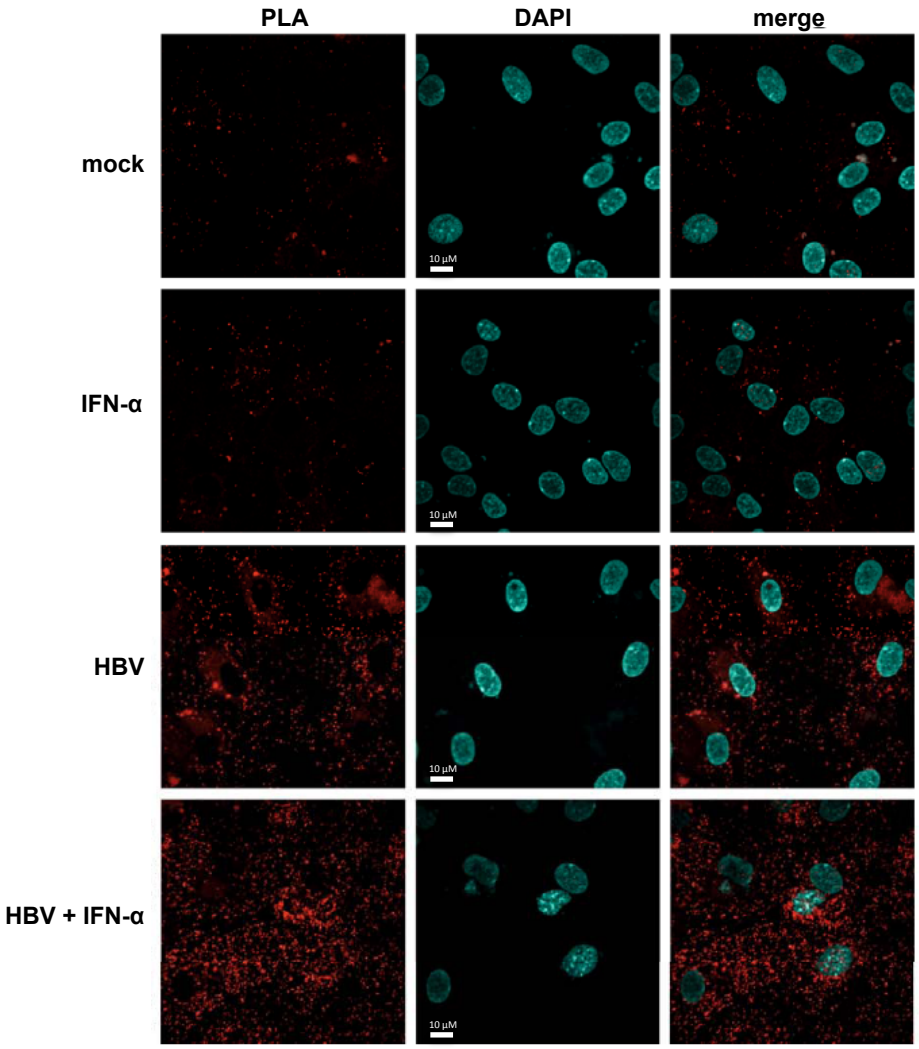

Figure S20. Proximity Ligation Assay (PLA) staining in HepaRG cells with antibodies against HBc and A3A. Imaging was done by spinning disc microscopy and single cells were identified based on DAPI staining. PLA spots were automatically counted with a fixed threshold in all measurements.

A

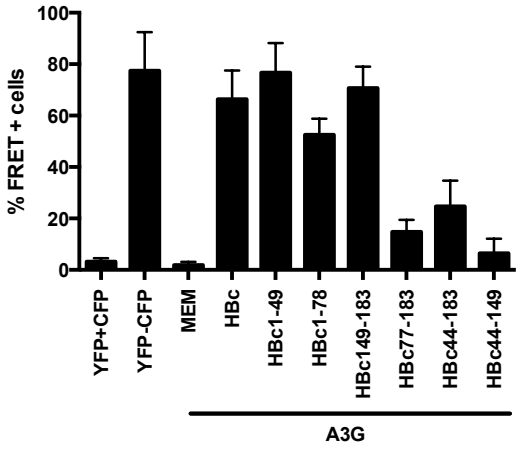

B

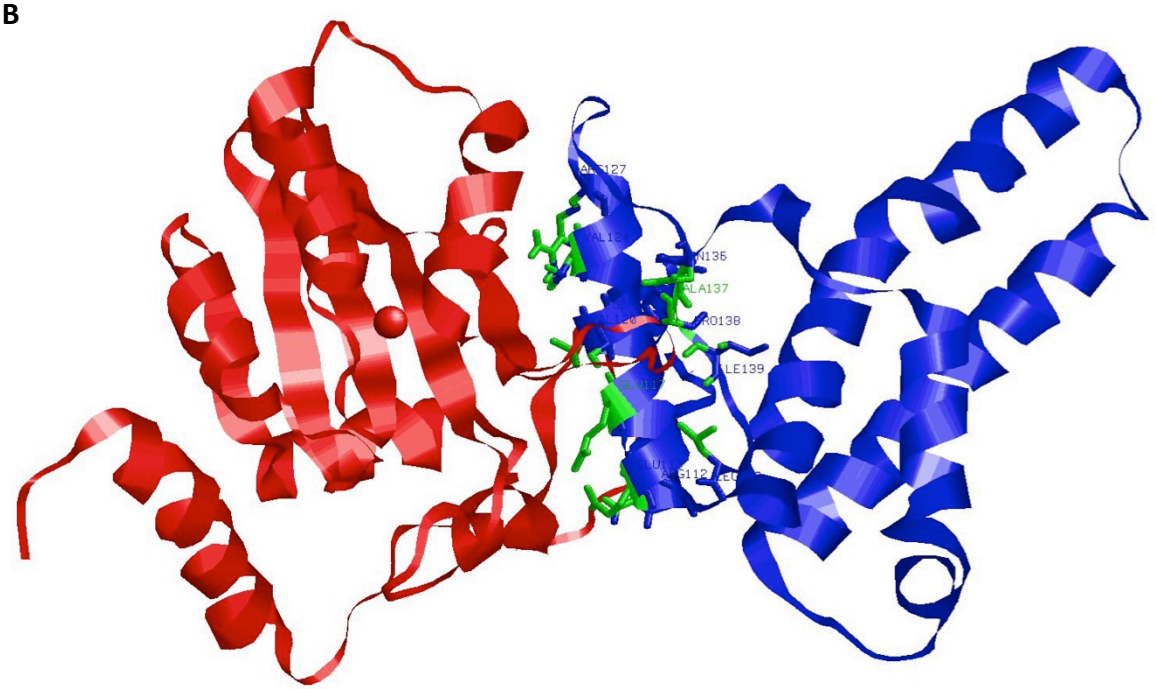

Figure S21. (A) Interaction of serial HBV Core (HBc)-YFP deletion mutants with A3G-CFP assessed by FACS-FRET in Huh7.5 hepatoma cells. Indicated are percentages of cells scoring FRET positive for each co-transfection. CFP-only and YFP-only as well as co-transfection of a highly membrane incorporated MEM fusion protein served as negative controls. A CFP-YFP fusion protein was used as positive control. Mean values and standard deviations were calculated from three to four independent experiments. **(B)** The potential interaction sites of modeled A3A (red) and HBV core protein (blue) are depicted: amino acids of HBV core locating within a distance of 3.1 Å from A3A, which are mainly located at residues 110 to 149, are highlighted in green indicating interaction. The red ball indicates the zinc atom embedded in the catalytic site of A3A. Our model indicates an interaction of HBV core α-helix 4 with A3A.

Table S1: **Treatment of humanized uPA/SCID mice with LTβR agonists.**

mouse*	treatment	total intracellular HBV DNA (copies/ cell)	cccDNA (copies/cell)
1	hu-IgG	570	1,79
2	hu-IgG	599	3,51
3	CBE11	84	0,84
4	CBE11	105	0,96

*Humanized uPA/SCID mice were infected with HBV and treated with chlodronate two times (day 0 and 5) to deplete murine liver macrophages and avoid Fc-receptor mediated killing of transplanted human hepatocytes. At day three, mice were treated either with LTβR agonistic antibody CBE11 or with control human IgG. Mice were sacrificed at day 10 and HBV rc and cccDNA in livers were analyzed.